Plant YTHDF proteins are direct effectors of antiviral immunity against an *N6*-methyladenosine-containing RNA virus

Mireya Martínez-Pérez[1] (ID), Frederic Aparicio[1] (ID), Laura Arribas-Hernández[2] (ID),
Mathias Due Tankmar[2] (ID), Sarah Rennie[2] (ID), Sören von Bülow[2], Kresten Lindorff-Larsen[2] (ID),
Peter Brodersen[2,*] (ID) & Vicente Pallas[1,**] (ID)

Abstract

In virus–host interactions, nucleic acid-directed first lines of defense that allow viral clearance without compromising growth are of paramount importance. Plants use the RNA interference pathway as a basal antiviral immune system, but additional RNA-based mechanisms of defense also exist. The infectivity of a plant positive-strand RNA virus, alfalfa mosaic virus (AMV), relies on the demethylation of viral RNA by the recruitment of the cellular *N6*-methyladenosine (m^6A) demethylase ALKBH9B, but how demethylation of viral RNA promotes AMV infection remains unknown. Here, we show that inactivation of the Arabidopsis cytoplasmic YT521-B homology domain (YTH)-containing m^6A-binding proteins ECT2, ECT3, and ECT5 is sufficient to restore AMV infectivity in partially resistant *alkbh9b* mutants. We further show that the antiviral function of ECT2 is distinct from its previously demonstrated function in the promotion of primordial cell proliferation: an *ect2* mutant carrying a small deletion in its intrinsically disordered region is partially compromised for antiviral defense but not for developmental functions. These results indicate that the m^6A-YTHDF axis constitutes a novel branch of basal antiviral immunity in plants.

Introduction

Viruses are intracellular pathogens that use their genetic code to turn cells into their multiplication factories. To defend against hostile takeover by viral genetic material, host organisms have evolved mechanisms to recognize foreign nucleic acids. For example, bacteria use a combination of restriction-modification and CRISPR-Cas systems to eliminate viral nucleic acids (Barrangou *et al*, 2007; Loenen *et al*, 2014; Egido *et al*, 2022), and a combination of cyclic nucleotide signaling and NAD⁺ depletion systems coupled to nucleic acid sensors to eliminate infected cells from a population (Tal *et al*, 2021; Koopal *et al*, 2022). Similar basal antiviral immune systems operating directly on viral nucleic acids have been found in animals, where at least four distinct cytoplasmic systems recognize double-stranded features of viral RNA to activate signaling pathways that lead to the induction of innate antiviral immune responses (Wu & Chen, 2014; Rehwinkel & Gack, 2020; Holleufer *et al*, 2021; Slavik *et al*, 2021). In plants, the double-strandedness of cytoplasmic viral RNA is also used to distinguish it from endogenous RNA, since plants use RNA interference (RNAi) as a potent basal antiviral defense mechanism (Lindbo, 2012). In addition, extracellular double-stranded RNA (dsRNA) can be sensed by as yet unidentified receptors to effect antiviral pattern-triggered immunity PTI (Meier *et al*, 2019; Niehl & Heinlein, 2019). The effectiveness of RNAi as a basal antiviral defense mechanism is illustrated by the fact that nearly all plant viruses use anti-RNAi effectors as virulence factors (Voinnet *et al*, 1999; Csorba *et al*, 2015; Jin *et al*, 2021). In plants, RNAi remains the most generally employed basal antiviral defense mechanism to date, but features of viral genetic material other than its double-stranded regions may be used for distinction between cellular and viral RNA, and hence, for antiviral defense. For example, in both mammals and plants, the non-sense-mediated mRNA decay (NMD) pathway may detect and repress long viral RNAs with stop codons of reading frames located towards the 5′-end of the viral transcript (Balistreri *et al*, 2014; Garcia *et al*, 2014), a feature that viruses may circumvent either through the use of anti-NMD factors or by organizing their genomes into a long poly-protein-encoding mRNA containing only a single downstream stop codon (Balistreri *et al*, 2014; Popp *et al*, 2020). Furthermore, in the

1 Instituto de Biología Molecular y Celular de Plantas, Consejo Superior de Investigaciones Científicas, Universitat Politècnica de València, Valencia, Spain
2 Department of Biology, University of Copenhagen, Copenhagen, Denmark
*Corresponding author. Tel: +45 35322031; E-mail: pbrodersen@bio.ku.dk
**Corresponding author. Tel: +34 963877877; E-mail: vpallas@ibmcp.upv.es

nematode *Caenorhabditis elegans* that also relies on RNAi for basal antiviral defense (Gammon, 2017), a terminal uridyltransferase exerts antiviral immunity independently of RNAi, although the feature of viral RNA recognized in this case remains unclear (Le Pen *et al*, 2018).

Covalent modification of mRNA is now understood to play important roles in the regulation of gene expression, and many viruses contain modified nucleotides of importance for the outcome of the host–virus interaction (Gokhale & Horner, 2017; Courtney, 2021). The most widespread, and probably most important, modification of eukaryotic cellular mRNA is N^6-methyladenosine (m^{6}A) (Arribas-Hernández & Brodersen, 2020; Wiener & Schwartz, 2021). m^{6}A is installed at DRACH (D = A/G/U, R = G/A, H = A/C/U) or GGAU motifs in pre-mRNA by a dedicated, nuclear multi-subunit methyltransferase, or "writer," complex (Arribas-Hernández & Brodersen, 2020; Arribas-Hernández *et al*, 2021a). This highly conserved complex consists of a heterodimeric catalytic core of methyltransferase-like proteins known as MAC, and a large MAC-associated complex (MACOM) required for activity *in vivo* (Bokar *et al*, 1994, 1997). In Arabidopsis, MAC consists of MTA (AT4G10760, orthologous to metazoan Mettl3) and MTB (AT4G09980, orthologous to metazoan Mettl14), while MACOM is composed of several factors, including FKBP12 INTERACTING PROTEIN 37 (FIP37, AT3G54170, orthologous to metazoan WTAP), VIRILIZER (VIR, AT3G05680), the ubiquitin ligase HAKAI (AT5G01160), and the Zn-finger protein HAKAI-INTERACTING Zn-FINGER2 (HIZ2; AT5G53440, equivalent to metazoan ZC3H13/ Flacc; Zhong *et al*, 2008; Shen *et al*, 2016; Růžička *et al*, 2017; Zhang *et al*, 2022a). m^{6}A can be demethylated, or "erased," by a set of enzymes belonging to the AlkB family of Fe(II)- and α-ketoglutarate-dependent dioxygenases (Van den Born *et al*, 2009) that comprises 14 members in Arabidopsis (Mielecki *et al*, 2012; Kawai *et al*, 2014). Demethylation activity has been demonstrated experimentally for ALKBH9B and ALKBH10B (Mielecki *et al*, 2012; Kawai *et al*, 2014; Duan *et al*, 2017; Martínez-Pérez *et al*, 2017), and recent evidence suggests its presence also in ALKBH9C (Amara *et al*, 2022).

It is an important function of m^{6}A to generate a binding site for RNA-binding proteins specialized for the m^{6}A recognition via a so-called YT521-B homology (YTH) domain (Imai *et al*, 1998; Stoilov *et al*, 2002; Zhang *et al*, 2010; Dominissini *et al*, 2012; Liao *et al*, 2018). The YTH domain contains an aromatic cage that forms a hydrophobic pocket for the methyl group in m^{6}A, thus resulting in 10–20-fold higher affinity for m^{6}A-containing RNA than for unmethylated RNA (Li *et al*, 2014; Luo & Tong, 2014; Theler *et al*, 2014; Xu *et al*, 2014, 2015; Zhu *et al*, 2014; Patil *et al*, 2018). For that reason, YTH domain proteins are sometimes referred to as m^{6}A readers. In the cytoplasm, a family of so-called YTHDF proteins binds to m^{6}A-containing RNA, and while genetics shows these YTHDF proteins to be of key importance for plant and animal development (Arribas-Hernández *et al*, 2018, 2020; Kontur *et al*, 2020; Lasman *et al*, 2020), the exact reasons for this biological importance remain undefined in plants, and heavily debated in mammals (Tsutsui & Higashiyama, 2017; Lasman *et al*, 2020; Murakami & Jaffrey, 2022). In the flowering plant Arabidopsis, there are 11 YTHDF proteins, named EVOLUTIONARILY CONSERVED C-TERMINAL REGION (ECT) because of the presence of the conserved YTH domain in the C-terminal part, after an N-terminal intrinsically

disordered region (IDR) as in YTHDF proteins of other organisms. ECT2 and ECT3 act redundantly as m^{6}A readers to stimulate cellular proliferation in organ primordia, such that *ect2/ect3* double mutants show delayed leaf and flower formation, slow root and stem growth, and aberrant leaf, flower, silique, and trichome morphology (Arribas-Hernández *et al*, 2018, 2020, 2021b). In nearly all cases, these phenotypes are exacerbated by additional mutation of *ECT4* (Arribas-Hernández *et al*, 2018, 2020), and five additional Arabidopsis YTHDF proteins (ECT5, ECT6, ECT7, ECT8, ECT10) share the molecular functions of ECT2/3 required for primordial cell proliferation, as seen by complementation of *ect2/ect3/ect4* phenotypes upon ectopic expression in the ECT2/3 expression domain (preprint: Flores-Téllez *et al*, 2023). Stimulation of growth is a recurrent function of plant YTHDF proteins because similar roles have been found for rice and tomato YTHDF proteins (Ma *et al*, 2022; Yin *et al*, 2022), and because the sole YTHDF protein of the liverwort *Marchantia polymorpha* can replace ECT2/3 function when expressed in Arabidopsis (preprint: Flores-Téllez *et al*, 2023).

m^{6}A is also found in viral mRNAs, first seen as early as 1975 in simian virus 40 mRNAs (Lavi & Shatkin, 1975). Subsequent studies have shown the presence of m^{6}A in viral RNAs from several mammalian RNA and DNA viruses (Williams *et al*, 2019; Wu *et al*, 2020; Baquero-Perez *et al*, 2021), and direct binding of YTH proteins to RNAs from some of these viruses, such as hepatitis C virus (HCV), zika virus (ZIKV) or human immunodeficiency virus-1 (HIV-1) has been demonstrated (Gokhale *et al*, 2016; Kennedy *et al*, 2016; Lichinchi *et al*, 2016). In plant viruses, fewer examples of the involvement of m^{6}A in infection cycles have been described (van den Born *et al*, 2008; Martínez-Pérez *et al*, 2017, 2021; Tian *et al*, 2021; Zhang *et al*, 2021, 2022b; He *et al*, 2023).

We previously showed that viral RNA of several positive-strand RNA viruses contains m^{6}A (Martínez-Pérez *et al*, 2017), among them alfalfa mosaic virus (AMV), which consists of three genomic RNA molecules (RNA1, RNA2, and RNA3) and a subgenomic RNA (RNA4; Bujarski *et al*, 2019). Importantly, AMV infectivity of wild-type Arabidopsis plants depends on the activity of a cellular m^{6}A demethylase, ALKBH9B (Martínez-Pérez *et al*, 2017; Alvarado-Marchena *et al*, 2021), since local and systemic AMV infections are attenuated in *alkbh9b* knockout plants, including a nearly complete block of viral invasion of the floral stems that is possibly explained by the severely reduced ability of AMV to enter into the vascular tissue of *alkbh9b* mutants (Martínez-Pérez *et al*, 2017, 2021). Thus, methylation of the viral RNA is part of an important defense mechanism that the infectious virus adapts to by manipulation of ALKBH9B to act on the viral RNA (Martínez-Pérez *et al*, 2017, 2021). This defense mechanism seems to affect some of the steps of the viral replication cycle, because, in addition to local and systemic movement, clear differences in AMV levels were also detected upon infection of protoplasts isolated from wild-type and *alkbh9b* mutant plants (Martínez-Pérez *et al*, 2021). It is at present unclear whether reduced AMV titers in infected cells underlie all effects on systemic infection in *alkbh9b* mutants, or whether the hypermethylation of AMV RNA in *alkbh9b* mutants affects additional steps specifically linked to systemic movement. Most importantly, the molecular basis of m^{6}A-dependent antiviral defense remains undefined. It may, for example, involve m^{6}A-binding reader proteins or RNA structure properties related to altered base pairing properties of m^{6}A-U compared with A-U, the latter perhaps suggested by the observation that

adenosines in a DRACH context within the 3′UTR of alfalfa mosaic virus (AMV) RNA 3 represent a key structural requirement for viral replication (Alvarado-Marchena et al, 2022).

Here, we show that mutation of the *ECT2/ECT3/ECT4/ECT5* module in Arabidopsis reduces AMV resistance, and that the increased AMV resistance of *alkbh9b* mutants can be reverted by mutation of *ECT2/ECT3/ECT5*. We also show that the functions of ECT2 in the stimulation of cellular proliferation and antiviral defense can be separated by a small deletion in its N-terminal IDR. These results establish the m^6A-YTHDF axis as a novel basal antiviral defense layer.

Results

AMV infection induces components of the m^6A-YTH axis

To guide the genetic dissection of m^6A-mediated defense against AMV, we first analyzed transcriptome changes upon AMV infection with particular attention to transcripts encoding components of the m^6A pathway. For this experiment, we selected young, emerging rosette leaves of infected plants, since m^6A-binding proteins and methyltransferase subunits were shown to be mostly expressed in tissues with high cell division rates (Zhong et al, 2008; Arribas-Hernández et al, 2018, 2020). Differential expression analysis showed that 2,611 genes were significantly upregulated ($\log_2FC \geq 1$; FC, fold change), whereas only 194 genes were downregulated ($\log_2FC \leq -1$) during AMV infection (Fig 1A). Molecular functions among differentially expressed genes were enriched in protein–protein interaction and DNA- or RNA-binding activities (Fig 1B). This set also included some components of the m^6A machinery (Fig 1C). The levels of mRNAs encoding three components of the methylation complex— *MTA*, *MTB*, and *VIR*—were upregulated by the infection, whereas the levels of mRNAs encoding potential m^6A erasers did not substantially change (Fig 1C). Among YTHDF-encoding genes, only *ECT5* showed a greater than 2-fold upregulation (Fig 1C). We verified the induction of *ECT5*, along with that of *MTA*, *MTB*, and *VIR*, using quantitative RT–PCR analysis (Fig 1D). The previously described m^6A readers ECT2 and ECT3 (Arribas-Hernández et al, 2018) were also significantly upregulated, albeit with smaller effect size ($\log_2FC$ values 0.6 and 0.4 for *ECT2* and *ECT3*, respectively; Fig 1C).

ECT2, ECT3, ECT4, and ECT5 are implicated in AMV resistance

We next analyzed single *ect2-1*, *ect3-1*, *ect4-2* mutants (Arribas-Hernández et al, 2018), and an *ect5* T-DNA insertion mutant (*ect5-1*, SALK_131549; Fig EV1A and B) for possible defects in AMV resistance (Appendix Table S1). No single mutants showed significant differences in AMV titers (Fig EV1C), perhaps due to functional redundancy as demonstrated for their growth-promoting functions (Arribas-Hernández et al, 2020). We therefore analyzed composite mutants of *ECT2*, *ECT3*, and *ECT4*. The viral RNA levels in inoculated leaves (local infection) were slightly higher in mutant combinations involving *ect2* but reached statistical significance only in the *ect2-1/ect3-1/ect4-2* (henceforth, *te234*) triple mutant (Fig 2A). However, these differences were much more evident in noninoculated leaves (systemic infection), in which AMV titers were clearly elevated in *ect2-1/ect3-1* (henceforth, *de23*) and *te234* mutant plants compared with wild-type (Fig 2B). Double mutants involving *ect4* showed

weak, if any, effects on AMV accumulation, while *te234* tended to have somewhat higher AMV titers than *de23*, although this effect was variable in size between experiments (Fig 2B and Appendix Fig S1B). The differences in systemic viral load between wild-type and *ect2/ect3* double knockouts were confirmed using an *ect2/ect3* double mutant with independent knockout alleles (*ect2-3/ect3-2*, Appendix Fig S1 and Table S1; Arribas-Hernández et al, 2018). Next, since *ECT5* is tightly linked to *ECT2* (Fig EV2A), we used CRISPR-Cas9 to produce the double *ect2-1/ect5-2* (*de25*) and triple *ect2-1/ect3-1/ect5-4* (*te235*) mutants (Fig EV2B). Importantly, we observed increased AMV titers in noninoculated tissues of *de25* compared with wild-type (Fig 2C and D), pointing to an important involvement of ECT5 in limiting systemic AMV infection. In contrast to *de23* mutants, *de25* mutants exhibited no obvious leaf morphology defects or delay in leaf formation (Fig 2E). As observed for the *te234* mutants, *te235* tended to show moderately higher AMV titers systemically than *de23*, although with some variability between experiments (Fig 2D and Appendix Fig S1C). Similar results were obtained with different CRISPR-induced *ect5* alleles (Appendix Fig S2 and Table S1). We draw several conclusions from these initial genetic analyses. First, several ECT proteins impact the outcome of infection of Arabidopsis by AMV. Second, similar to modulation of the m^6A content in AMV RNA by inactivation of *ALKBH9B*, effects in both inoculated and noninoculated tissues can be observed upon mutation of *ECT* genes, suggesting that the mechanism of m^6A-dependent antiviral defense may involve ECT proteins. We note that several factors may underlie the fact that much clearer differences were observed in uninoculated young tissue compared with inoculated mature leaves, including the fact that ECT2/3/4 are mostly expressed in rapidly dividing, young tissue (Arribas-Hernández et al, 2018, 2020) and their absence, therefore, has a greater effect in these tissues. Third, ECT2, ECT3, and ECT5 are required for systemic resistance to AMV, observable in *ect2/ect3* and *ect2/ect5* mutants, while ECT4 seems to have a minor role as its effect is mostly observable as a variable enhancement of the increased susceptibility of *ect2/ect3* double knockout mutants in noninoculated aerial tissues.

Because of the nearly universal role of RNAi as a basal defense mechanism against plant RNA viruses, we next addressed the potential implication of this mechanism in the case of AMV. RNAi relies on three enzymatic activities: dsRNA synthesis by RNA-dependent RNA polymerases (RDRs), in particular RDR6, dsRNA processing into small RNA by DICER-LIKE (DCL) ribonucleases, and small RNA-guided target repression by ARGONAUTE (AGO) proteins. Because of pronounced genetic redundancy among AGO paralogs in their antiviral activity, and because mutation of the important antiviral protein AGO1 leads to strong developmental defects due to the implication of AGO1 in microRNA function (Vaucheret et al, 2004; Baumberger & Baulcombe, 2005; Qi et al, 2005; Wang et al, 2011; Brosseau & Moffett, 2015), we initially focused on RDR6, its cofactor SGS3, and the DCLs DCL4 and DCL2 that are all known to be important for basal defense against many viruses (Lopez-Gomollon & Baulcombe, 2022). Mutants with lesions in *RDR6/SGS3*, *DCL4*, or *DCL2* did not show significant changes in AMV levels in noninoculated leaves at 7 days postinoculation (dpi; Fig EV3A), a point in time in which the effect of ECTs on infection is evident. We next analyzed the role of the ECTs when RNAi is attenuated. We chose the inactivation of *RDR6* in the *de23* background, since cucumber mosaic virus, another m^6A-containing positive-strand RNA virus
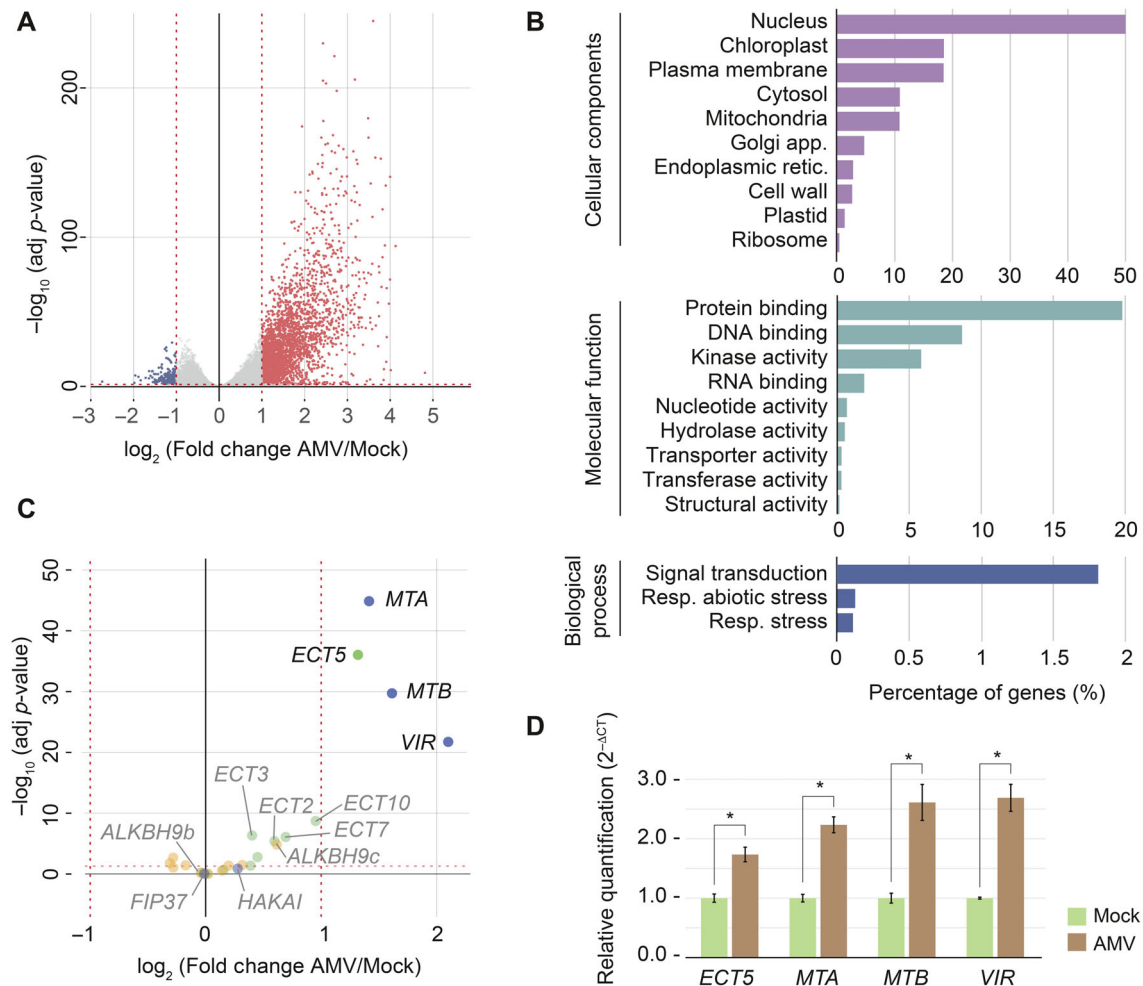
Figure 1. Differential gene expression analysis between mock and AMV-infected *Arabidopsis* plants at 8 days postinoculation.

A   Volcano plot depicting differential expression of nearly 18,000 unique genes (minimum expression of 1 read per kilobase per million, RPKM) in response to AMV infection. In red, upregulated genes ($log_2FC \geq 1$; adjusted P-value ≤ 0.05); in blue, downregulated genes ($log_2FC \leq -1$; adjusted P-value ≤ 0.05).

B   Most highly enriched gene ontology (GO) terms in the set of differentially expressed genes.

C   Filtered volcano plot visualizing the expression of genes involved in the m⁶A pathway in response to AMV infection.

D   RT-qPCR analysis of expression of four upregulated m⁶A pathway-related genes in response to AMV infection (three biological replicates). Error bars represent the standard error of the mean (SEM). Asterisks indicate a $P < 0.05$ applying the Student's t-test for ΔCt mean values ($n = 3$).

Source data are available online for this figure.

phylogenetically related to AMV, is silenced predominantly by the RDR6-dependent viral siRNAs (Dalmay *et al*, 2000; Mourrain *et al*, 2000; Wang *et al*, 2011; Martínez-Pérez *et al*, 2017). Even in the *rdr6* mutant background, inactivation of *ECT2/ECT3* led to increased AMV titers (Fig EV3B), and, thus, we conclude that the action of m⁶A-ECT system is independent of RNAi. These results do not, however, rule out that RNAi may affect the outcome of AMV infection in some settings of the virus–plant interaction, for instance with different strengths of inoculum or at different times postinoculation.

The m⁶A-binding activity of ECT2 is required for its antiviral activity

The amino acid residues of human YTHDF proteins implicated in RNA and m⁶A binding are highly conserved in Arabidopsis ECT proteins (Fray & Simpson, 2015; Scutenaire *et al*, 2018). This includes in particular the three tryptophan residues that form the m⁶A-binding aromatic cage. Mutational studies of these tryptophan residues have demonstrated that integrity of the aromatic cage is required for ECT2 binding to m⁶A-modified RNAs (Scutenaire *et al*, 2018) and for ECT2, ECT3, and ECT4 function *in vivo* (Arribas-Hernández *et al*, 2018, 2020). Thus, to test whether ECT-mediated antiviral resistance requires the m⁶A-binding activity, we used *de23* mutants expressing either ECT2^WT-mCherry or the m⁶A-binding deficient point mutant ECT2^W464A-mCherry (Appendix Table S1). The ECT2^W464A-mCherry-expressing lines were clearly defective in AMV resistance, while expression of ECT2^WT-mCherry in *de23* restored resistance to levels comparable to that of wild-type or *ect3-1* (Fig 3A, upper and lower panels show two independent complementing transgenic lines).
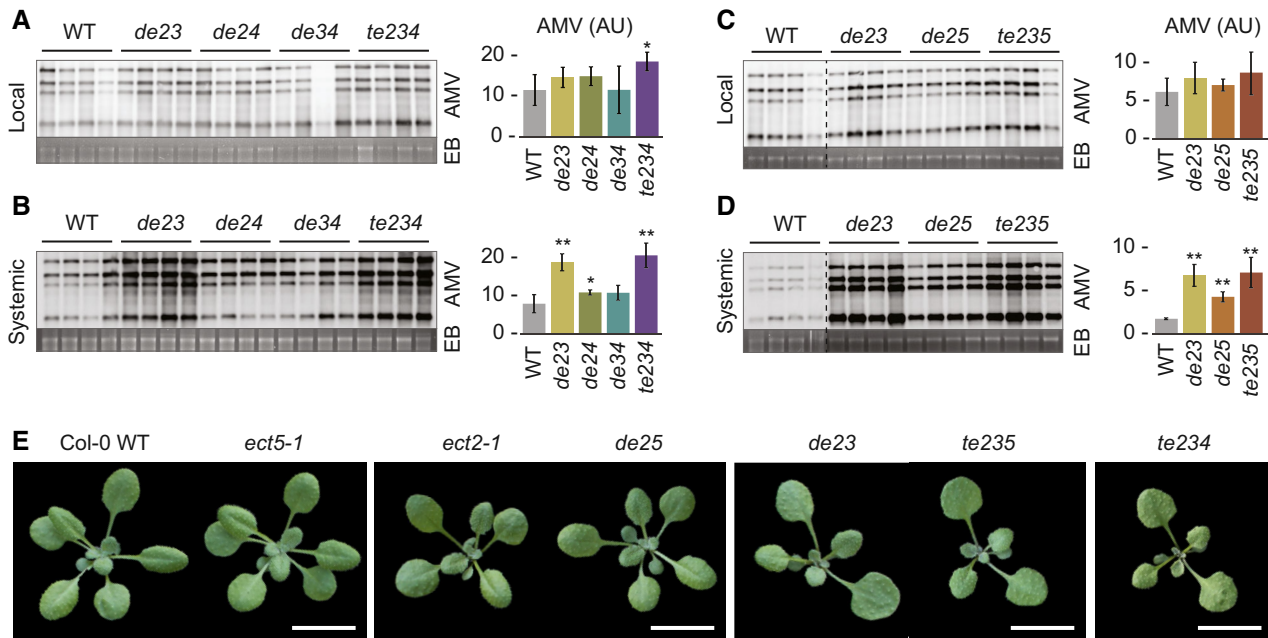
Figure 2. Combined inactivation of *ECT2/3/4/5* enhances titers of AMV in systemic tissues.

A–D RNA blots were hybridized to AMV-specific probes to reveal accumulation of viral RNA in double (de) and triple (te) ect2/3/4 (A, B) or ect2/3/5 (C, D) mutants compared with wild-type (WT) plants. A and C show local infection at 3 days postinoculation (dpi); B and D show systemic infection in aerial tissue at 7 dpi. Each panel shows a representative RNA blot displaying AMV RNAs 1–4 (left) and its quantification histogram (right). Dashed lines indicate noncontiguous samples analyzed on the same membrane. Ethidium bromide staining of ribosomal RNAs (EB) was used as RNA loading control. Error bars indicate standard deviations. Asterisks indicate significant differences from the WT (*: $P < 0.05$; **: $P < 0.01$) using the Student's t-test ($n = 4$). AU, arbitrary units.

E Phenotypes of rosettes of the indicated genotypes at 19 days after germination. Scale bars: 1 cm.

Source data are available online for this figure.

We note that the loss of AMV resistance in both knockout and ECT2[W464A]-mCherry-expressing lines could in principle be an indirect consequence of the developmental defect of *ect* mutants that may render the plant more amenable to viral replication, rather than a direct effect of missing or defective association with m⁶A-containing viral RNA. We disfavor this possibility for two reasons. First, in contrast to *de23*, *de25* mutants display no obvious rosette phenotype (Fig 2E), yet the increase in AMV titers compared with wild-type is robust (Fig 2D). Second, the mutation of the nuclear m⁶A writer component *VIR* causes a rosette phenotype similar to, but slightly stronger than *ect2/ect3/ect4* (Růžička *et al*, 2017), yet does not lead to the same degree of loss of antiviral resistance (Fig 3B).

ECT2 associates with AMV RNA *in vivo*

We next sought to establish whether ECTs associate with AMV RNA, focusing specifically on ECT2 due to its higher expression levels compared with ECT3 and ECT5 (Arribas-Hernández *et al*, 2021b). We used the proximity-labeling method HyperTRIBE (Targets of RNA-binding proteins Identified by Editing; McMahon *et al*, 2016), in which the catalytic domain of the fly Adenosine Deaminase Acting on RNA (ADAR) is fused to ECT2 and expressed under the control of the ECT2 promoter. Because adenosine-to-inosine editing by ADAR is detected as A-to-G transitions by RNA-Seq, RNA bound by ECT2 can be identified by virtue of its higher A-G

editing proportions compared with control lines expressing unfused ADAR (McMahon *et al*, 2016; Xu *et al*, 2018; preprint: Rennie *et al*, 2021). Using an experimental set-up similar to our previous HyperTRIBE analysis, which faithfully identified direct endogenous mRNA targets of ECT2 and ECT3 (Arribas-Hernández *et al*, 2021a, 2021b), we employed five independent transgenic lines expressing either the ECT2-FLAG-ADAR fusion or the free FLAG-ADAR (Appendix Table S1), the latter acting as negative controls. The negative control lines showed on average higher FLAG-ADAR expression levels than the ECT2-FLAG-ADAR fusion lines (Fig 4A), contributing to higher stringency in the analysis. In contrast, viral titers were generally lower in these same lines, thus providing fewer sequenced reads for the viral RNAs (Fig 4B). Nearly all detected AMV sequence reads mapped to the positive strand, as expected (Fig 4C). We first selected 395 candidate positions showing A-G changes compared with the reference AMV sequence in at least two of five lines. Since the viral RNA-dependent RNA polymerase introduces random mutations, and since free ADAR has a nonzero background editing activity, we sought to formally test whether significantly higher editing proportions were observed in ECT2-FLAG-ADAR lines compared with FLAG-ADAR control lines. For this purpose, we employed our recently published method for the analysis of HyperTRIBE data (preprint: Rennie *et al*, 2021). This statistical analysis identified two sites in the positive strand of RNA2 (RNA2_701 and RNA2_2271) showing consistent A-G changes across FLAG-ADAR fusion lines, with modeled editing
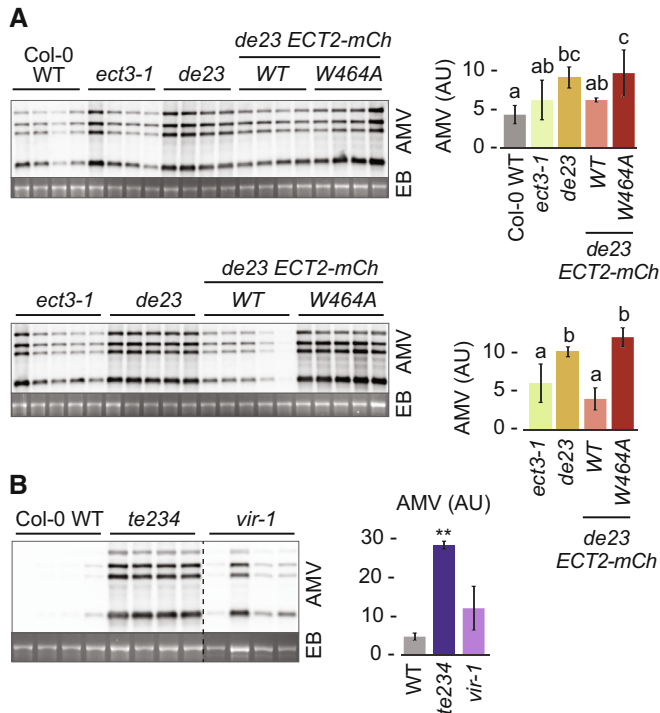
Figure 3. ECT-mediated defense against AMV requires intact m⁶A-binding pockets and is not an indirect effect of a dysfunctional m⁶A-ECT axis.

A, B RNA-blot analysis of AMV systemic infection in plants expressing ECT2[WT]-mCherry (WT) or ECT2[W464A]-mCherry (W464A) in the *de23* background (A) and in *vir-1* plants (B) at 7 days postinoculation. Each panel shows a representative RNA blot displaying AMV RNAs 1–4 (left) and its quantification histogram (right). Ethidium bromide staining of rRNAs (EB) was used as RNA loading control. Genotypes are indicated on the top of each northern blot. In (A) upper and lower panels show independent complementation transgenic lines, and different letters indicate statistical differences according to Fisher's least significant difference (LSD; $P < 0.05$). In (B) the dashed line indicates noncontiguous samples that are analyzed on the same membrane. Error bars indicate standard deviations. Asterisks indicate significant differences from the WT (**: $P < 0.01$) applying the Student's t-test ($n = 4$). AU, arbitrary units.

Source data are available online for this figure.

proportions significantly higher than in FLAG-ADAR control lines (FDR < 0.05, Fig 4D). We further noted an additional likely *bona fide* site on RNA1 (RNA1_2482), which did not make it under the FDR threshold, likely due to a lack of power resulting from low editing proportions. In all three cases, editing proportions in the ECT2-FLAG-ADAR fusion lines correlated strongly with corresponding ECT2-FLAG-ADAR expression levels across the five individual transgenic lines used as replicates (Figs 4E and EV4), supporting the conclusion that these A-G changes are a result of editing by the ECT2-FLAG-ADAR fusion. Finally, we noted that, while the fused ADAR to ECT2 is not expected to act on the exact binding site, the two high-confidence sites in RNA2 did appear in the vicinity of DRACH motifs, which may be indicative of the methylated position to which ECT2 was recruited (Fig 4F and G). Taken together, our HyperTRIBE data indicate that ECT2 associates with AMV RNA *in vivo*.

The m⁶A-ECT axis constitutes a basal layer of antiviral defense

The observations that inactivation of *ECT2/3/(4)/5* leads to higher AMV infectivity, that ECT2 associates with AMV RNA *in vivo*, and that its antiviral effect requires an intact m⁶A-binding site are consistent with a model in which binding of ECTs to methylated viral RNA causes inhibition of viral replication. However, the results reported thus far suffer from the limitation that they do not analyze the true effect of ECT association with AMV RNA, because they are carried out with a wild-type virus in an otherwise wild-type Arabidopsis genetic background. Since AMV requires the endogenous demethylase ALKBH9B, probably recruited via its capsid protein (CP) to AMV RNA, for infectivity (Martínez-Pérez *et al*, 2017), these experiments address the influence of ECTs on infection in a setting in which a virulence mechanism is diminishing the impact of adenosine methylation of viral RNA. Because the CP has multiple essential functions in the infection cycle, including RNA encapsidation and initial translational control (Herranz *et al*, 2012), informative genetic manipulation of the CP is not straightforward. By contrast, our previous study showed that the systemic infection in the floral stems is nearly fully blocked upon disruption of the host *ALKBH9B* gene. We therefore constructed *alkbh9b/te235* mutants (Appendix Table S1) to test the impact of *ECT* inactivation in a setting in which AMV infectivity is strongly incapacitated due to hypermethylation. The AMV titers in *alkbh9b/te235* were intermediate between *alkbh9b* and *te235* at early stages of infection (7 dpi; Fig 5A) but were identical to *te235* (and Col-0) at late stages (20 dpi; Fig 5B), where little to no AMV was detectable in *alkbh9b*. We interpret these results to mean that m⁶A-ECTs efficiently limit the speed of systemic spread of AMV to the point where nearly no virus accumulates in stems upon leaf inoculation in *alkbh9b* (Fig 5B; Martínez-Pérez *et al*, 2017, 2021), even at late stages of infection. At such late points, additional aspects of the host–AMV interaction are likely to limit AMV titers to a maximal value reached by both Col-0 and *te235*. Although spreading and systemic accumulation is lower in *alkbh9b/te235* than in *te235*, the virus eventually reaches these same maximal titers systemically, in marked contrast to what is observed in *alkbh9b*. Importantly, therefore, the inactivation of *ECT2/3/5* is sufficient to break the strong m⁶A-based protection against systemic infection in the absence of ALKBH9B, clearly showing that ECT2/3/5 are requisite effectors of the m⁶A-based defense against AMV. These results argue that for AMV, and perhaps other viruses whose RNA is *N6*-adenosine methylated, the m⁶A-ECT axis constitutes a basal layer of antiviral defense that must be overcome for the virus to be infectious. Indeed, the results conceptually parallel the restoration of infectivity of RNA virus strains with defective anti-RNAi effectors by inactivation of the RNAi machinery (Deleris *et al*, 2006; Wang *et al*, 2011).

The growth-promoting and antiviral activities of ECT2 are genetically separable

The model of basal antiviral defense mediated by m⁶A-ECT2/3/4/5 may be at odds with the described endogenous function of these factors in promoting cellular proliferation (Arribas-Hernández *et al*, 2020), as a highly metabolically active state favors viral replication. Thus, it is difficult to imagine how the same biochemical activity would promote both antiviral defense and cellular proliferation. We
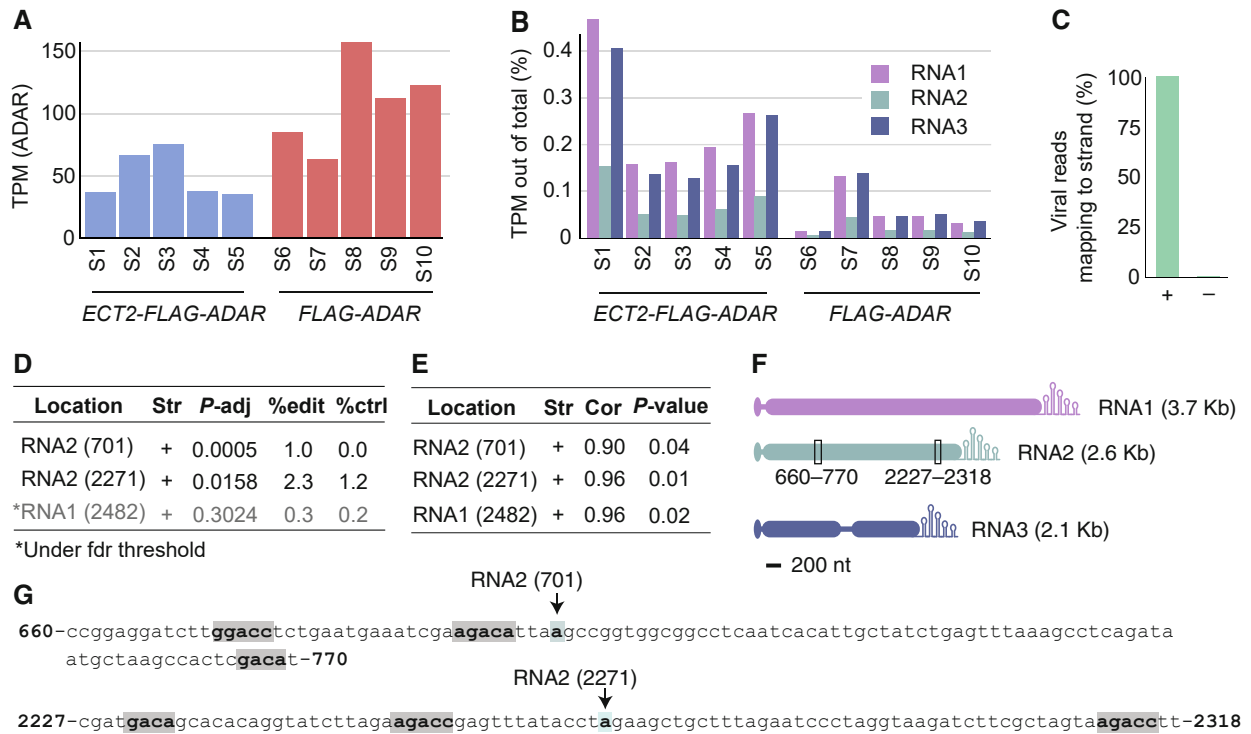
Figure 4. HyperTRIBE identifies *in vivo* interactions between ECT2 and AMV RNAs.

A   ADAR expression (TPM—Transcripts Per Kilobase Million—mapping) in five samples of ECT2-FLAG-ADAR (S1–S5) and FLAG-ADAR (S6–S10) transgenic lines.
B   Percentage of total reads mapping to the AMV RNAs in the different samples.
C   Percentage of reads mapping to either the positive or negative AMV strand.
D   Positions preferentially edited in AMV RNAs of the ECT2–FLAG-ADAR compared with FLAG-ADAR lines. %edit and %ctrl show the mean editing proportion (G/(A + G)) in the ECT2-FLAG-ADAR and FLAG-ADAR lines, respectively. Significant sites were determined using hyperTRIBER pipeline (preprint: Rennie *et al*, 2021). To be formally tested, an A-to-G change had to be present in at least two of the five ECT2-FLAG-ADAR samples.
E   Correlation between ADAR log TPM and editing proportions across individual ECT2-FLAG-ADAR transgenic lines for the three most highly significantly edited sites.
F   Schematic representation of the positions of the two high-confidence ECT2-dependent editing sites in AMV RNAs.
G   Exact position of the two high-confident ECT2-dependence editing sites in AMV RNA2 (light blue). The DRACH motives located nearby editing sites are highlighted in gray.

Source data are available online for this figure.

therefore reasoned that ECTs may use different biochemical and/or biophysical properties to achieve both effects. To analyze this possibility, we made use of a series of small deletions engineered in the long N-terminal intrinsically disordered region (IDR). These deletions were originally designed to identify regions of importance for the developmental function of ECT2 (preprint: Tankmar *et al*, 2023). Of six ~50–80 aa deletions, four had no effect on leaf formation (preprint: Tankmar *et al*, 2023). Since Tyr residues may promote IDR-driven phase separation (Wang *et al*, 2018; Martin *et al*, 2020; Bremer *et al*, 2022), we selected the ECT2$^{\Delta N5}$ mutant carrying a deletion in a Tyr-rich region present in many ECTs for analysis of AMV resistance (Figs 6A, and EV5A and B). We observed a reduction in AMV resistance in transgenic lines expressing ECT2$^{\Delta N5}$-mCherry compared with ECT2^{WT}-mCherry in the *te234* mutant background (Fig 6B). This effect was reproducible, albeit somewhat variable, across several transgenic lines with similar levels of ECT2-mCherry or ECT2$^{\Delta N5}$-mCherry (Fig 6C). Because the rate of leaf formation and leaf morphology in *te234* lines expressing ECT2$^{\Delta N5}$-mCherry were indistinguishable from those expressing ECT2^{WT}-mCherry (Figs 6D and E, and EV5C), yet AMV resistance was measurably compromised, these

results suggest that the IDR of ECT2 harbors two separable activities employed to achieve different goals: one that stimulates cellular proliferation by binding to endogenous m^{6}A-containing mRNA, and one that effects basal antiviral resistance when ECT2 binds to hypermethylated viral RNA. We note that since the antiviral activity was not fully abolished in *te234* expressing ECT2$^{\Delta N5}$-mCherry, we cannot formally exclude the possibility that the different impacts of this mutation on antiviral defense and developmental phenotypes are caused by a threshold effect, such that the same reduction in molecular activity would give rise to a measurably reduced antiviral, but not developmental, function of ECT2. A complete resolution of this issue requires a full understanding of the precise molecular nature of both ECT2 functions, a task not achieved for functions of any YTHDF protein to date. Nonetheless, regardless of the exact interpretation of the reduced antiviral resistance in *te234* lines expressing ECT2$^{\Delta N5}$-mCherry, this result reinforces the conclusion reached from infections of *de25* and *vir-1* mutants that compromised antiviral resistance in *ect* mutants is not simply an indirect effect of developmental defects caused by dysfunction of the m^{6}A-ECT axis.
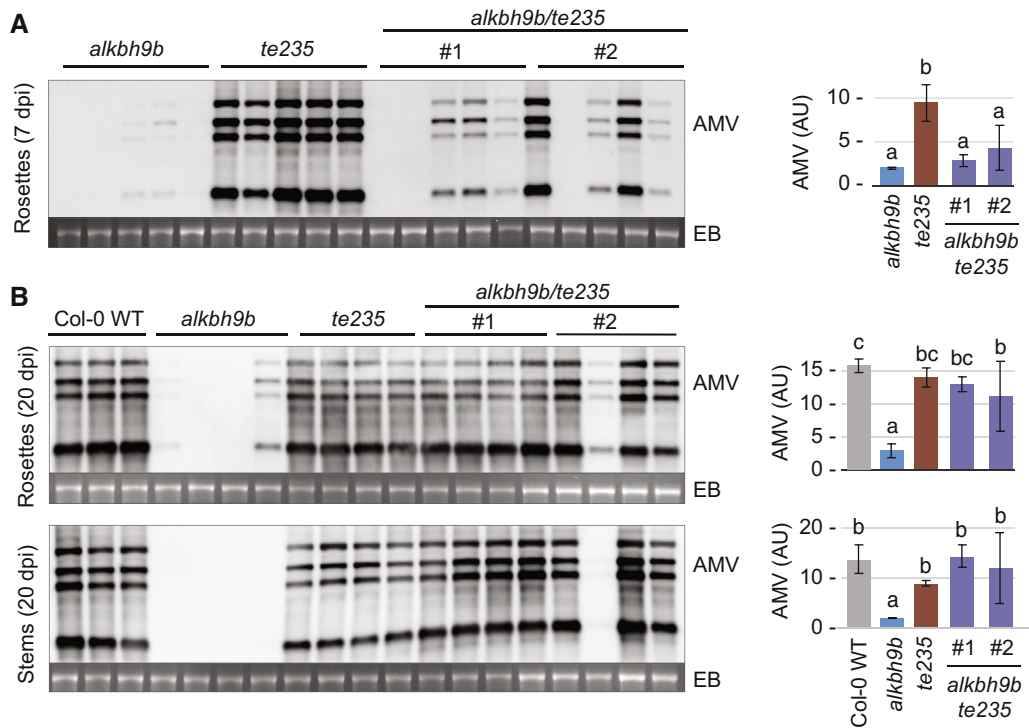
Figure 5. The ECT2/3/5 module constitutes a basal defense layer against AMV infection, since knockout of ECT2/3/5 in the *alkbh9b* background recovers susceptibility.

A, B Systemic infection of rosettes at 7 days postinoculation (dpi) (A) or rosettes and floral stems at 20 dpi (B). Each panel shows a representative RNA blot displaying AMV RNAs 1–4 (left) and its quantification histogram (right). Ethidium bromide staining of rRNAs (EB) was used as RNA loading control. Genotypes are indicated on the top of each northern blot. #1 and #2 correspond to the progeny of two different quadruple homozygous F2 siblings derived from the *alkbh9b* x *te235* cross. Error bars show standard deviations. AU, arbitrary units. Different letters indicate statistical differences according to Fisher's least significant difference (LSD; *P* < 0.05).

Source data are available online for this figure.

The region deleted in ECT2 $^{\Delta N5}$ contributes to the propensity of ECT2 to phase separate

We next investigated the possibility that the relevance of the region deleted in ECT2$^{\Delta N5}$ for AMV resistance may be linked to the propensity to engage in higher-order assemblies for two reasons. First, ECT2 clearly has a propensity to form condensate-like structures *in vitro* and *in vivo* (Arribas-Hernández *et al*, 2018), with localization to cytoplasmic stress granules upon abiotic stress (Scutenaire *et al*, 2018). Second, as noted above, the region deleted in ECT2$^{\Delta N5}$ is enriched in Tyr residues that may be drivers of phase separation (Wang *et al*, 2018; Martin *et al*, 2020; Bremer *et al*, 2022). Thus, we carried out molecular simulations to probe and quantify the propensity of the IDR of ECT2 and ECT2$^{\Delta N5}$ to self-associate in a phase-separated state using a recently published coarse-grained model that accurately captures the phase-separation behavior of IDRs (Tesei *et al*, 2021). These simulations confirmed that the IDR of ECT2 has a clear propensity to phase separate, similar to, albeit less pronounced than, the well-studied IDRs of the human RNA-binding proteins hnRNPA1 and FUS (Fig 7). Importantly, the IDR of ECT2$^{\Delta N5}$ showed substantially reduced propensity to phase separate compared with that of ECT2, with clear signs of dispersion over time in the simulations (Fig 7A and B), and a thermodynamically less

favorable transition to the condensed phase (Fig 7C). A simulation of the behavior of an IDR of ECT2 in which all Tyr residues in the $\Delta N5$ region had been substituted by Ala (ECT2$^{9xY \rightarrow A}$) further indicated the essential contribution of the Tyr residues in this region for phase separation (Fig 7), potentially explaining their conservation in ECT2 orthologs and ECT paralogs more broadly. Taken together, our genetic dissection of the IDR of ECT2, and our simulation of its biophysical properties suggest that the ability to phase separate or form other higher-order structures may be of particular importance for the antiviral function of ECT2.

Discussion

A new basal antiviral defense mechanism

Our analysis of the AMV–Arabidopsis interaction provides a clear case of the m6A-YTHDF axis acting as a basal antiviral defense layer: when the infection mechanism targeting the m6A-YTHDF axis is hampered by host *ALKBH9B* mutation, AMV systemic infection is severely disrupted and practically blocked in floral stems. However, systemic infectivity is restored upon additional mutation of *ECT2*, *ECT3*, and *ECT5*. These genetic data resemble the key arguments for
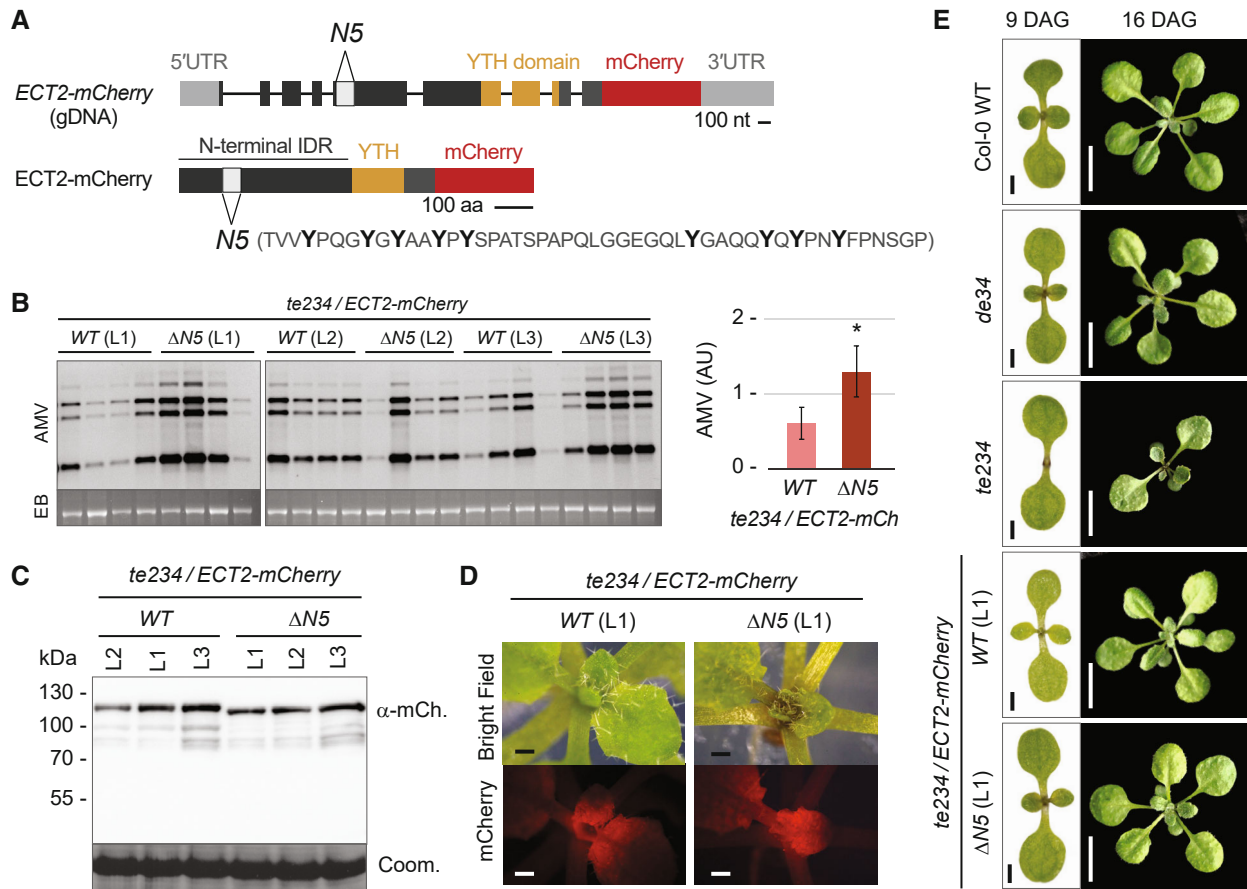
Figure 6. A Tyr-rich region of ECT2 IDR is necessary for antiviral but not for developmental functions of the protein.

A Schematic representations of the annotated ECT2 gene (AT3G13460.1, top) or protein (bottom) showing the deletion of the Tyr-rich region (ΔN5) in ECT2^{ΔN5}-mCherry lines.

B AMV systemic infection at 7 days postinoculation of three independent complementation lines (L1-3) expressing ECT2-mCherry or ECT2^{ΔN5}-mCherry in the *te234* background. Left, a representative RNA blot displaying AMV RNAs 1–4; right, the quantification histogram showing the mean of the three ECT2^{WT}-mCherry wild-type (WT) or ECT2^{ΔN5}-mCherry (ΔN5) lines. Ethidium bromide staining of rRNAs (EB) was used as RNA loading control. Error bars indicate standard deviations. AU, arbitrary units. Asterisk indicates significant differences from the WT (*: $P < 0.05$) applying the Student's t-test ($n = 3$).

C Protein blot developed with mCherry antisera to show accumulation of ECT2^{WT}-mCherry or ECT2^{ΔN5}-mCherry fusion proteins in pools of the same samples used in panel (B). Proteins on the membrane were stained with Coomassie blue as loading control (lower panel).

D Fluorescence microscopy of the second pair of true leaves of plants expressing ECT2^{WT}-mCherry or ECT2^{ΔN5}-mCherry in the *te234* background as indicated. Scale bars: 1 mm.

E Phenotypes of seedlings and young rosettes of the indicated genotypes at 9 and 16 days after germination (DAG). Scale bars: black, 1 mm; white, 1 cm.

Source data are available online for this figure.

the importance of RNAi as a basal antiviral defense mechanism in plants and insects (Deleris *et al*, 2006; Ding & Voinnet, 2007). Apart from obvious mechanistic questions that we touch on below, this discovery raises the important question of how widespread the use of this defense mechanism may be. AMV may be a special case, as it is one of only very few studied plant RNA viruses for which no anti-RNAi effector has been identified, and indeed prunus necrotic ring-spot virus (PNRSV), a virus genetically and functionally closely related to AMV (Pallas *et al*, 2013), does not induce easily detectable siRNAs, unlike nearly all other studied plant RNA viruses (Herranz *et al*, 2015). In addition, we could not detect a contribution of some key RNAi factors to defense against AMV systemic invasion at the same time postinoculation in which ECTs play an important role. The more interesting possibility, that the m^{6}A-ECT axis has

widespread use as an antiviral defense mechanism should not be disregarded, however. A study comparing the Arabidopsis transcriptome in response to 11 plant viruses pointed out that differential expression of *ECT3* is a common response to all viruses, while the genes encoding the methylase components MTA and HAKAI1 and the YTHDF proteins ECT5 and ECT6 were differentially expressed upon infection with at least one virus (Postnikova & Nemchinov, 2012). This suggests that the m^{6}A pathway is more generally implicated in plant–virus interactions. Clearly, it will be of key importance to analyze the degree to which RNA of other plant viruses contain m^{6}A, what the effect of inactivation of genes encoding the major YTHDF proteins is on their infectivity, and whether they too employ mechanisms to interfere with the m^{6}A-YTHDF axis. We note in this regard that studies on mammalian viruses have shown the
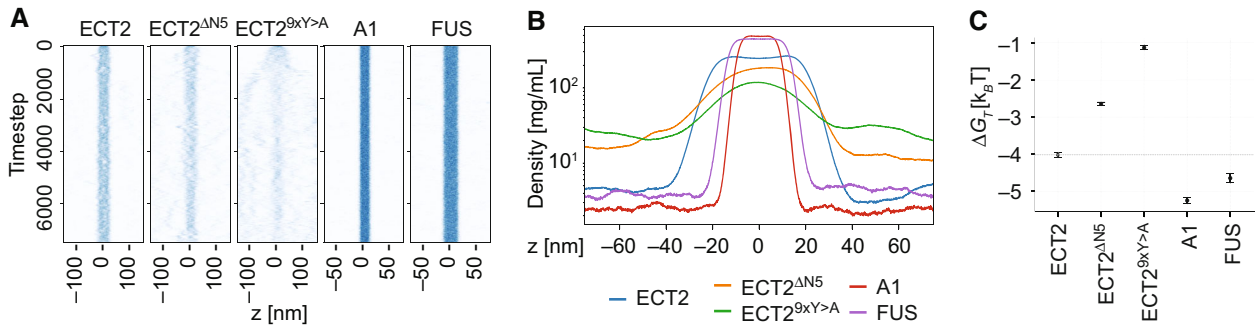
Figure 7. The region deleted in ECT2$^{\Delta N5}$ contributes substantially to phase separation of the IDR of ECT2.

A   Simulation of the tendency of the IDRs of ECT2, ECT2$^{\Delta N5}$, ECT2$^{9xY\rightarrow A}$, as well as those of human hnRNPA1 (A1) and FUS to remain in condensed phase or disperse in solution over time.
B   Time-averaged density profiles for the simulations shown in (A).
C   Calculated free energy change for the transition between aqueous solution and condensed phase. Error bars indicate standard errors from block averaging across each simulation using the BLOCKING tool (github.com/fpesceKU/BLOCKING).

widespread implication of the m⁶A-YTHDF axis in animal–virus interactions, albeit not with the rigorous genetics employed here to demonstrate function as a basal layer of defense. For example, the depletion of mammalian YTHDF proteins was found to enhance viral replication of ZIKV (Lichinchi et al, 2016) and HIV-1 (Tirumuru et al, 2016; Jurczyszak et al, 2020), and to increase stability and protein expression of hepatitis B virus (HBV; Imam et al, 2018) and endogenous retroviral mRNAs (Chelmicki et al, 2021). The m⁶A-YTHDF system is not universally employed for antiviral defense in animals, however, as viruses also appear to manipulate it for their benefit. For example, mammalian YTHDF proteins stimulate HIV-1 Gag processing and viral release (Tirumuru et al, 2016), and enhance viral translation and replication via binding to m⁶A sites located in the 3′UTR of the viral RNAs (Kennedy et al, 2016). The difficulty of generalizing the role of m⁶A in viral RNA in host–virus interactions is well illustrated by several examples. In HBV, m⁶A in the 5′-UTR of viral pregenomic RNA enhances reverse transcription, while m⁶A sites located in the 3′-UTR promote RNA destabilization (Imam et al, 2018). In addition, the recent characterization of the wheat m⁶A writer MTB as a susceptibility factor in the interaction with wheat yellow mosaic virus shows that, also in plants, m⁶A in viral RNA cannot automatically be assumed to be antiviral (Zhang et al, 2022b).

Are all m⁶A effects on AMV infectivity mediated by YTHDF proteins?

The marked restoration of AMV infectivity of alkbh9b mutants upon inactivation of ECT2, ECT3, and ECT5 strongly argues that YTHDF proteins are the major, if not the exclusive, effectors of m⁶A-mediated basal AMV defense. In general, at 7 dpi, knockout of ECT2/3/5 in the alkbh9b background leads to intermediate viral loads compared with alkbh9b and ect2/ect3/ect5 mutants, although the outcome shows some variability. However, the most plausible explanation for this is that, in a hypermethylation context—where ALKBH9B is not functional—residual contributions by some of the remaining ECT proteins become relevant. Nonetheless, YTHDF-independent effects of m⁶A cannot be formally excluded at this point. For example, m⁶A may act as a secondary structure switch

caused by altered m⁶A-U compared with A-U base pairs (Kierzek & Kierzek, 2003; Liu et al, 2015), a property that may either benefit or impede viral replication. An evaluation of this potentially important possibility will require mapping of m⁶A sites in AMV to single-nucleotide resolution in alkbh9b and wild-type backgrounds, as well as in vivo secondary structure analysis now feasible via sequencing-adapted methods (Poulsen et al, 2015).

Source of adenosine methylation of AMV RNA

The observation that the infectivity of AMV is not drastically enhanced in vir-1 mutants, in contrast to te234, constitutes strong evidence that the hypersusceptibility of composite ect mutants is not simply an indirect consequence of developmental defects in plants with a disabled m⁶A-YTHDF pathway. This important conclusion is reinforced by the hypersusceptibility of ect2/ect5 mutants and of te234 mutants expressing ECT2 with the ΔN5 deletion, as both of these backgrounds do not show developmental delay and aberrant leaf morphology. VIR is required for adenosine methylation of endogenous mRNA (Růžička et al, 2017), but if it were also the case for AMV RNA, a hypersusceptibility phenotype would be expected, thus arguing that methylation of AMV RNA is largely VIR-independent. Such a scenario would be consistent with the cytoplasmic replication cycle of AMV, but nuclear localization of MAC/MACOM proteins in uninfected plants. It does, therefore, raise the pertinent question of what the identity of the AMV RNA methyl transferase is. We see two possible explanations. Either AMV RNA methylation is carried out by an unidentified cytoplasmic adenosine methyltransferase, or, perhaps more likely, certain MAC/MACOM subunits translocate to the cytoplasm during AMV infection, as has been reported in different infection contexts in mammalian cells (Hao et al, 2019; Srinivas et al, 2021; Sacco et al, 2022), and, more recently, also in plants (Zhang et al, 2022b).

Distinction between cellular and viral m⁶A-containing RNA and the basis of ECT-mediated antiviral defense

At first glance, it is a surprising result that ECT2/ECT3 carry out functions in both antiviral defense and in the stimulation of cellular

proliferation, especially given that endogenous mRNA targets of ECT2/ECT3 are enriched in factors involved in central metabolic processes such as oxidative phosphorylation and translation (Arribas-Hernández *et al*, 2021b). Thus, ECT2/ECT3 binding to endogenous targets presumably increases their expression, consistent with the predominant downregulation of ECT2/ECT3 mRNA targets in root meristem cells devoid of ECT2/ECT3/ECT4 activity (Arribas-Hernández *et al*, 2021b). By contrast, AMV RNA is repressed by ECT2/ECT3/(ECT4)/ECT5. What could dictate the different outcomes of binding of these proteins to endogenous mRNA versus AMV RNAs? As a working model to explain our results, we propose that m^6A site multiplicity in AMV RNA may be a key factor distinguishing it from endogenous mRNA. Closely spaced m^6A sites in *cis* occupied by multiple ECT proteins would lead to high local concentrations of the IDRs, thus potentially driving the formation of a biomolecular condensate, and sequestration from the translation machinery. Such repression would not occur on endogenous mRNAs if they tend only to harbor single m^6A sites, as multivalent interactions are key drivers of condensates. In this setting, the YTHDF proteins may use short linear motifs in their IDRs to recruit other cellular factors to enhance protein expression, but such activities would be overridden upon condensation into a separate phase. Although admittedly speculative at this point, this model is consistent with a number of observations. First, abiotic stress indeed causes ECT2, ECT3, and ECT4 to condense into separate cytoplasmic bodies (Arribas-Hernández *et al*, 2018), identified as stress granules in the case of ECT2 in plants subjected to heat stress (Scutenaire *et al*, 2018), and purified ECT2 can separate into regularly shaped hydrogel-like particles *in vitro* (Arribas-Hernández *et al*, 2018). Thus, ECT2 has a marked propensity to self-associate. Second, our simulations show that the phase-separation propensity of the IDR of ECT2 is substantially reduced in the ECT2$^{\Delta N5}$ mutant. Third, mammalian YTHDF2 has only weak phase-separation properties *in vitro*, but they are markedly stimulated upon binding to RNA that contains multiple, but not single, m^6A sites (Gao *et al*, 2019; Ries *et al*, 2019; Fu & Zhuang, 2020). Fourth, a recent computational approach to infer RNA modifications in plant-pathogenic viruses using high-throughput annotation of modified ribonucleotides (HAMR), a software that predicts modified ribonucleotides using high-throughput RNA sequencing data, revealed a higher proportion of RNA chemical modifications in comparison with mRNAs of Arabidopsis (Marquez-Molins *et al*, 2022). Finally, we note that although multiple m^6A sites have been found in many endogenous mRNA targets in Arabidopsis, it is unclear whether they co-exist on the very same mRNA molecules. We stress that despite the existence of evidence consistent with the proposed model for the basis of m^6A-YTHDF-mediated basal AMV defense, we view this model as a conceptual framework of value in the design of future experiments to test its validity.

Materials and Methods

Plant growth conditions, virus inoculation, and northern blot analysis

The source and background of each *Arabidopsis thaliana* (Columbia-0) transgenic line are described in Appendix Table S1. Plants were grown in 6 cm diameter pots in a growth chamber with a photoperiod of 25°C-16 h light/20°C-8 h dark. The mechanical inoculations of 15–19 days old plants were carried out using carborundum and purified virions (1 mg/ml) of AMV PV0196 isolate (Plant Virus Collection, DSMZ) in PE buffer (30 mM sodium phosphate buffer, pH 8). Next, the detection of vRNAs was performed by northern blot analysis. Inoculated leaves and noninoculated aerial tissue were harvested at the corresponding dpi. Systemic infection was evaluated in single plants, while local viral accumulation was analyzed by pooling two plants per sample. Tissues were grounded in liquid nitrogen with mortar and pestle and total RNA was extracted, following EXTRAzol reagent protocol (Blirt; Gdańsk, Poland), from 0.1 g leaf material. For northern blots, 500 ng of total RNA was denatured by formaldehyde treatment and after agarose gel electrophoresis in MOPS buffer, RNAs were transferred to positively charged nylon membranes (Roche; Basel, Switzerland) by capillarity in SSC buffer as previously described (Sambrook *et al*, 1988) and hybridized with digoxigenin-labeled riboprobes to detect AMV RNA 1, RNA 2, RNA 3 and sgRNA 4. Synthesis of the digoxigenin-labeled riboprobes, hybridization, and digoxigenin-detection procedures was performed as previously described (Pallás *et al*, 1998). Hybridization intensity signal was measured on files from Fujiflm LAS-3000 Imager using Fujiflm Image Gauge V4.0. Every infection experiment was repeated at least twice.

Generation of Arabidopsis CRISPR/Cas9 transgenic lines

Arabidopsis lines carrying CRISPR/Cas9-mediated gene knockout were generated using the pKAMA-ITACHI Red (pKIR1.1) vector as previously described with some modifications (Tsutsui & Higashiyama, 2017). Different oligonucleotides (Appendix Table S2) were designed inside the ORF of ECT5 (AT3G13060), searching for protospacer adjacent motif (PAM) sequences (NGG), to work as sgRNAs. Then, ligations of the hybridized DNA oligomers with the vector, previously digested with AarI enzyme, were performed. *Agrobacterium tumefaciens* GV3101 was transformed with the resulting vectors, and cultures expressing two different sgRNAs were used to generate Arabidopsis stable transgenic lines by floral dip transformation (Clough & Bent, 1998) in *ect2-1* and *de23* backgrounds. Selection of T1 transgenic plants was carried out by hygromycin resistance and a first assortment of Cas9-free T2 seeds was performed by the absence of red fluorescence. Final genotyping by PCR with specific primers (Appendix Table S2) was realized from T2 plants and confirmed in T3 transformants. Finally, an RT–PCR with specific primers (Appendix Table S2) of total RNA extraction from plants of selected lines and the sequencing of the cDNA products verified the frameshift mutations (Fig EV2C and D).

Generation of Arabidopsis ECT2$^{\Delta N5}$-mCherry lines

Cloning and line selection of ECT2$^{\Delta N5}$-mCherry was performed by USER cloning and agrobacterium-mediated transformation as described in Tankmar (preprint: Tankmar *et al*, 2023). In brief, USER-compatible primers (LA336, MT5, MT6, LA337) were used to amplify fragments from *ECT2Pro:ECT2gDNA-mCherry:ECT2Ter*; a construct previously generated by Arribas-Hernández *et al* (2018). The fragments were purified and inserted into pCAMBIA3300U (pCAMBIA3300 with a double PacI USER cassette inserted between the PstI-XmaI sites at the multiple cloning site; Nour-Eldin *et al*,

2006) after which the plasmid was transformed into *Escherichia coli* DH5α (NEB). Kanamycin-resistant colonies were selected and their plasmids purified followed by restriction digestion and sequencing prior to introduction into *Agrobacterium tumefaciens* GV3101 for plant transformation. Arabidopsis stable transgenic lines were generated by floral dip transformation (Clough & Bent, 1998) of *ect2-1/ect3-1/ect4-2* (*te234*) (Arribas-Hernández et al, 2018), and selection of primary transformants (T1) was done on MS-agar plates supplemented with glufosinate-ammonium (Merck, Darmstadt, Germany; 10 mg/l). T2 generation was used for the infection experiments.

RNA differential expression analysis between Arabidopsis Col-0 WT mock and AMV samples

Two-week Arabidopsis Col-0 wild-type (WT) plants were mechanically inoculated with 30 mM sodium phosphate buffer pH7 (mock treatment) or AMV PV0196 isolate viral particles in the same buffer. Tissues from the young, emerging rosette leaves were harvested at 8 dpi and ground in liquid nitrogen with mortar and pestle. Total RNA was extracted from 0.1 g leaf material using EXTRAzol reagent protocol (Blirt; Gdańsk, Poland) and treated with DNase I for 30 min at 37°C. The experiment consisted of three biological replicates (8 individual plants/replicate) of mock and AMV WT inoculated plants. Generation and sequencing of the cDNA libraries were performed by the Genomic Service (SCSIE) of the Universidad de Valencia. Six TruSeq Stranded cDNA libraries (three for healthy and three for AMV-infected plants) were sequenced by non-paired-end sequencing (75 bp) in a NextSeq 550 (Illumina; San Diego, CA, USA). The bioinformatics analysis was carried out by the Bioinformatic Service of IBMCP. DESeq2 package was the tool used for the differential expression analysis and an expression threshold of 1RPMK was applied.

Quantitative reverse transcription PCR (qPCR)

Four microliter of the reaction-containing DNA-free RNA were mixed with 0.5 μg (1 μl) of oligo(dT)18 (ThermoFisher Scientific; Waltham, MA, USA), denatured for 5 min at 65°C and added to a total of 20 μl of first-strand cDNA synthesis reaction containing 1 U of RevertAid H Minus Reverse Transcriptase, 0.5 U of Ribolock, 4 mM dNTP mix and 1× RT buffer (ThermoFisher Scientific). The RT reaction proceeded at 42°C for 1 h, followed by 10 min at 70°C to deactivate the enzyme. qPCR reactions were carried out using PyroTaq EvaGreen mix Plus (ROX; CulteK Molecular Bioline, Madrid, Spain) according to the manufacturer's instructions. All analyses were performed in triplicate on an ABI 7500 Fast-Real Time qPCR instrument (Applied Biosystems, Waltham, MA, USA). Specific oligonucleotides efficiencies were tested by qPCR using 10-fold serial dilutions of the corresponding cDNA (Appendix Table S2). Expression analysis was performed by calculating the relative quantification (RQ) values with respect to the endogenous genes *F-BOX* and *PDF2* (Lilly et al, 2011) of three biological replicates. The Student's *t*-test was applied to ΔCt values for statistical analysis.

Fluorescence microscopy

Imaging of plants at the rosette stage was done using a Leica MZ16 F fluorescence stereomicroscope, as described by Arribas-Hernández et al (2018).

Analysis of ECT2–RNA$_{AMV}$ interaction by HyperTRIBE

Five independent lines expressing ECT2 fused to the catalytic domain of the adenosine deaminase acting on RNA (ADAR) on the *ect2-1* background and five control lines expressing only ADAR on wild-type background (Arribas-Hernández et al, 2021a) were inoculated at 16 days with AMV (McMahon et al, 2016; Xu et al, 2018). Tissue from the innermost, young rosette leaves of each line (10 plants per sample) was selected at 7 dpi and grounded in liquid nitrogen with mortar and pestle. After total RNA extraction, precipitation of nucleic acids was carried out with 3.75 M LiCl (−20°C, overnight) to avoid tRNA precipitation. Next, these samples were submitted to a ribosomal RNA depletion treatment and cDNA libraries were prepared with CORALL Total RNA-Seq Library Prep Kit. The libraries were sequenced by paired-end sequencing (150 pb) on an Illumina NEXTseq 550 platform with v2.5 flow cell (300 cycles). Libraries were first quality checked before being merged across lanes, then trimmed, duplicated, and mapped using the CORALL Total RNA-Seq integrated Data Analysis Pipeline. Quantifications of reads mapping to AMV and ADAR were done using Salmon (Patro et al, 2017) using paired-end stranded mode. Mapped .bam files were converted to reflect forward and reverse strands before processing using hyperTRIBER (preprint: Rennie et al, 2021): briefly, base counts were aggregated from reads for all positions containing at least one mismatch, which were subsequently filtered for viral positions containing putative A-G edits in at least two of five lines expressing ECT2-FLAG-ADAR. Three hundred ninety-five candidates were formally tested for the differential occurrence of the base G while adjusting for differences in both read coverage at the position for each condition and variation in the levels of the ECT2-FLAG-ADAR. The results were subsequently FDR corrected in R, and the R function cor.test was used to calculate Pearson's correlation between ADAR and editing proportions (A/(A + G)) in ECT2-FLAG-ADAR samples. All plots were produced in R (R Core Team, 2021).

Western blot analysis

Total protein was extracted homogenizing 0.1 g of tissue from 7 dpi infected plants (same samples used for northern blot analysis in Fig 6B) with three volumes of extraction buffer (0.4 M Tris–HCl pH 8.8, 2% SDS, 15% glycerol, 0.1 M DTT), and heat at 95°C for 10 min. After centrifugation, 5 μl of Laemmli 6× (0.3 M Tris–HCl pH 6.8, 10% SDS, 0.05% xylene cyanol/bromophenol blue, 15% β-mercaptoethanol) were added to 25 μl of each sample and loaded into a 10% SDS–PAGE gel. The electrophoresis was run at 100 V for around 2 h, and proteins were transferred to a PVDF membrane, previously activated with methanol, at 30 V and 4°C overnight. ECT2-mCherry protein was detected using the anti-mCherry antibody (ab183628, Abcam; Cambridge, UK) at dilution 1:10,000. Secondary antibody and detection procedure was carried out following the manufacturer's instructions (ECL™ Prime Western Blotting System, Merck; Darmstadt, Germany).

Molecular simulations

We performed implicit-solvent coarse-grained simulations of IDR solutions using the CALVADOS 2 forcefield (Tesei et al, 2021; Tesei & Lindorff-Larsen, 2023) which uses a representation of the protein

with one bead per residue. Beads of neighboring residues were linked by harmonic bonds with an equilibrium distance of 0.38 nm and force constant of 8,033 kJ/mol/nm^2. Nonbonded interactions were modeled with a hydropathy amino acid "stickiness" model, truncated at 2 nm (Tesei & Lindorff-Larsen, 2023). In addition, we used a truncated (rc = 4 nm) and shifted Debye–Hückel potential to model salt-screened electrostatic interactions. Simulations were performed using a Langevin integrator (γ = 0.01 ps^{-1}) with a 0.01 ps time step.

We used a previously described procedure (Dignon *et al*, 2018; Tesei & Lindorff-Larsen, 2023) to perform slab simulations of IDRs of ECT2 ^{WT}, ECT2 $^{\Delta5}$, ECT2 $^{9x\ Y\rightarrow A}$, hnRNPA1, and FUS. The sequence "ECT2 9x Y→A" has nine substitutions of tyrosine residues to alanine in region N5 of ECT2 IDR. All protein sequences are listed at https://github.com/KULL-Centre/_2023_martinez-perez-AMV-ECT. For each of the five different IDR sequences, we ran a slab simulation with 100 copies of the IDR, with simulation box sizes of 25 × 25 × 300 nm (ECT2 WT and variants) and 15 × 15 × 150 nm (hnRNPA1 and FUS). We carried out all simulations for 7,500 ns at T = 293 K and saved configurations every 1 ns. We considered the first 2,000 ns of each simulation as equilibration which was not used for analysis. In a postprocessing step, we centered the protein condensates in the z-dimension of the simulation box. We obtained dense phase and dilute phase concentrations (c_{dense} and c_{dilute}, respectively) by fitting the time-averaged concentration profiles to a hyperbolic function (Tesei *et al*, 2021). We calculated excess transfer free energies via $\Delta G_{trans} = RT \ln (c_{dilute}/c_{dense})$ (Benayad *et al*, 2021).

Data availability

RNA-Seq and HyperTRRIBE RNA-Seq data: PRJEB56577 (https://www.ebi.ac.uk/ena/browser/view/PRJEB56577).

Code to perform and analyze the molecular simulations is available via https://github.com/KULL-Centre/_2023_martinez-perez-AMV-ECT and https://github.com/KULL-Centre/CALVADOS.

Expanded View for this article is available online.

Author contributions

Mireya Martínez-Pérez: Conceptualization; data curation; formal analysis; investigation; visualization; methodology; writing – original draft; writing – review and editing. **Frederic Aparicio:** Conceptualization; supervision; investigation; writing – original draft; writing – review and editing. **Laura Arribas-Hernández:** Conceptualization; resources; data curation; formal analysis; supervision; investigation; methodology; writing – review and editing. **Mathias Due Tankmar:** Data curation; software; formal analysis; validation; investigation; methodology. **Sarah Rennie:** Data curation; software; formal analysis; methodology. **Sören von Bülow:** Resources; data curation; software; formal analysis; visualization; methodology. **Kresten Lindorff-Larsen:** Conceptualization; data curation; software; validation; investigation; writing – review and editing. **Peter Brodersen:** Conceptualization; resources; data curation; formal analysis; supervision; funding acquisition; validation; investigation; visualization; writing – original draft; project administration; writing – review and editing. **Vicente Pallas:** Conceptualization; supervision; funding acquisition; validation; investigation; writing – original draft; project administration; writing – review and editing.

Disclosure and competing interests statement

The authors declare that they have no conflict of interest.

References

Alvarado-Marchena L, Marquez-Molins J, Martinez-Perez M, Aparicio F, Pallas V (2021) Mapping of functional subdomains in the atALKBH9B m6A-demethylase required for its binding to the viral RNA and to the coat protein of alfalfa mosaic virus. *Front Plant Sci* 12: 701683

Alvarado-Marchena L, Martínez-Pérez M, R.-Úbeda J, Pallas V, Aparicio F (2022) Impact of the potential m6A modification sites at the 3′UTR of alfalfa mosaic virus RNA3 in the viral infection. *Viruses* 14: 1718

Amara U, Shoaib Y, Kang H (2022) ALKBH9C, a potential RNA m6A demethylase, regulates the response of *Arabidopsis* to abiotic stresses and abscisic acid. *Plant Cell Environ* 45: 3566−3581

Arribas-Hernández L, Brodersen P (2020) Occurrence and functions of m6A and other covalent modifications in plant mRNA. *Plant Physiol* 182: 79−96

Arribas-Hernández L, Bressendorff S, Hansen MH, Poulsen C, Erdmann S, Brodersen P (2018) An m^{6}A-YTH module controls developmental timing and morphogenesis in *Arabidopsis*. *Plant Cell* 30: 952−967

Arribas-Hernández L, Simonini S, Hansen MH, Paredes EB, Bressendorff S, Dong Y, Østergaard L, Brodersen P (2020) Recurrent requirement for the m6A-ECT2/ECT3/ECT4 axis in the control of cell proliferation during plant organogenesis. *Development* 147: dev189134

Arribas-Hernández L, Rennie S, Köster T, Porcelli C, Lewinski M, Staiger D, Andersson R, Brodersen P (2021a) Principles of mRNA targeting via the *Arabidopsis* m6A-binding protein ECT2. *Elife* 10: e72375

Arribas-Hernández L, Rennie S, Schon M, Porcelli C, Enugutti B, Andersson R, Nodine M, Brodersen P (2021b) The YTHDF proteins ECT2 and ECT3 bind largely overlapping target sets and influence target mRNA abundance, not alternative polyadenylation. *Elife* 10: e72377

Balistreri G, Horvath P, Schweingruber C, Zünd D, McInerney G, Merits A, Mühlemann O, Azzalin C, Helenius A (2014) The host nonsense-mediated mRNA decay pathway restricts mammalian RNA virus replication. *Cell Host Microbe* 16: 403–411

Baquero-Perez B, Geers D, Díez J (2021) From a to m6A: the emerging viral epitranscriptome. *Viruses* 13: 1049

Barrangou R, Fremaux C, Deveau H, Richards M, Boyaval P, Moineau S, Romero DA, Horvath P (2007) CRISPR provides acquired resistance against viruses in prokaryotes. *Science* 315: 1709–1712

Baumberger N, Baulcombe DC (2005) *Arabidopsis* ARGONAUTE1 is an RNA slicer that selectively recruits microRNAs and short interfering RNAs. *Proc Natl Acad Sci USA* 102: 11928–11933

Benayad Z, von Bülow S, Stelzl LS, Hummer G (2021) Simulation of FUS protein condensates with an adapted coarse-grained model. *J Chem Theory Comput* 17: 525–537

Bokar JA, Rath-Shambaugh ME, Ludwiczak R, Narayan P, Rottman F (1994) Characterization and partial purification of mRNA N6-adenosine methyltransferase from HeLa cell nuclei: internal mRNA methylation requires a multisubunit complex. *J Biol Chem* 269: 17697–17704

Bokar JA, Shambaugh ME, Polayes D, Matera AG, Rottman FM (1997) Purification and cDNA cloning of the AdoMet-binding subunit of the human mRNA (N6-adenosine)-methyltransferase. *RNA* 3: 1233–1247

Bremer A, Farag M, Borcherds WM, Peran I, Martin EW, Pappu RV, Mittag T (2022) Deciphering how naturally occurring sequence features impact the phase behaviours of disordered prion-like domains. *Nat Chem* 14: 196–207

Brosseau C, Moffett P (2015) Functional and genetic analysis identify a role for *Arabidopsis* ARGONAUTE5 in antiviral RNA silencing. *Plant Cell* 27: 1742–1754

Bujarski J, Gallitelli D, García-Arenal F, Pallás V, Palukaitis P, Krishna Reddy M, Wang A (2019) ICTV virus taxonomy profile: Bromoviridae. *J Gen Virol* 100: 1206–1207

Chelmicki T, Roger E, Teissandier A, Dura M, Bonneville L, Rucli S, Dossin F, Fouassier C, Lameiras S, Bourc'his D (2021) m6A RNA methylation regulates the fate of endogenous retroviruses. *Nature* 591: 312–316

Clough SJ, Bent AF (1998) Floral dip: a simplified method for agrobacterium-mediated transformation of *Arabidopsis thaliana*. *Plant J* 16: 735–743

Courtney DG (2021) Post-transcriptional regulation of viral RNA through epitranscriptional modification. *Cell* 13: e1006188

Csorba T, Kontra L, Burgyán J (2015) Viral silencing suppressors: tools forged to fine-tune host-pathogen coexistence. *Virology* 479–480: 85–103

Dalmay T, Hamilton A, Rudd S, Angell S, Baulcombe DC (2000) An RNA-dependent RNA polymerase gene in *Arabidopsis* is required for posttranscriptional gene silencing mediated by a transgene but not by a virus. *Cell* 101: 543–553

Deleris A, Gallago-Bartolome J, Bao J, Kasschau KD, Carrington JC, Voinnet O (2006) Hierarchical action and inhibition of plant dicer-like proteins in antiviral defense. *Science* 313: 68–71

Dignon GL, Zheng W, Kim YC, Best RB, Mittal J (2018) Sequence determinants of protein phase behavior from a coarse-grained model. *PLoS Comput Biol* 14: e1005941

Ding SW, Voinnet O (2007) Antiviral immunity directed by small RNAs. *Cell* 130: 413–426

Dominissini D, Moshitch-Moshkovitz S, Schwartz S, Salmon-Divon M, Ungar L, Osenberg S, Cesarkas K, Jacob-Hirsch J, Amariglio N, Kupiec M *et al* (2012) Topology of the human and mouse m6A RNA methylomes revealed by m6A-seq. *Nature* 485: 201–206

Duan H-C, Wei L-H, Zhang C, Wang Y, Chen L, Lu Z, Chen PR, He C, Jia G (2017) ALKBH10B is an RNA N^6-Methyladenosine demethylase affecting *Arabidopsis* floral transition. *Plant Cell* 29: 2995–3011

Egido JE, Costa AR, Aparicio-Maldonado C, Haas PJ, Brouns SJJ (2022) Mechanisms and clinical importance of bacteriophage resistance. *FEMS Microbiol Rev* 46: fuab048

Flores-Téllez D, Tankmar M, von Bülow S, Chen J, Lindorff-Larsen K, Brodersen P, Arribas-Hernández L (2023) Conservation and diversification of the molecular functions of YTHDF proteins. *bioRxiv* https://doi.org/10.1101/2022.10.19.512826 [PREPRINT]

Fray RG, Simpson GG (2015) The *Arabidopsis* epitranscriptome. *Curr Opin Plant Biol* 27: 17–21

Fu Y, Zhuang X (2020) m6A-binding YTHDF proteins promote stress granule formation by modulating phase separation of stress granule proteins. *Nat Chem Biol* 16: 955–963

Gammon DB (2017) *Caenorhabditis elegans* as an emerging model for virus-host interactions. *J Virol* 91: e00509-17

Gao Y, Pei G, Li D, Li R, Shao Y, Zhang QC, Li P (2019) Multivalent m6A motifs promote phase separation of YTHDF proteins. *Cell Res* 29: 767–769

Garcia D, Garcia S, Voinnet O (2014) Nonsense-mediated decay serves as a general viral restriction mechanism in plants. *Cell Host Microbe* 16: 391–402

Gokhale NS, Horner SM (2017) RNA modifications go viral. *PLoS Pathog* 13: e1006188

Gokhale NS, McIntyre ABR, McFadden MJ, Roder AE, Kennedy EM, Gandara JA, Hopcraft SE, Quicke KM, Vazquez C, Willer J *et al* (2016) N6-methyladenosine in flaviviridae viral RNA genomes regulates infection. *Cell Host Microbe* 20: 654–665

Hao H, Hao S, Chen H, Chen Z, Zhang Y, Wang J, Wang H, Zhang B, Qiu J, Deng F *et al* (2019) N6-methyladenosine modification and METTL3 modulate enterovirus 71 replication. *Nucleic Acids Res* 47: 362–374

He H, Ge L, Li Z, Zhou X, Li F (2023) Pepino mosaic virus antagonizes plant m6A modification by promoting the autophagic degradation of the m6A writer HAKAI. *aBIOTECH* https://doi.org/10.1007/s42994-023-00097-6

Herranz MC, Pallas V, Aparicio F (2012) Multifunctional roles for the N-terminal basic motif of alfalfa mosaic virus coat protein: nucleolar/cytoplasmic shuttling, modulation of RNA-binding activity, and virion formation. *Mol Plant Microbe Interact* 25: 1093–1103

Herranz MC, Navarro JA, Sommen E, Pallas V (2015) Comparative analysis among the small RNA populations of source, sink and conductive tissues in two different plant-virus pathosystems. *BMC Genomics* 16: 117

Holleufer A, Winther KG, Gad HH, Ai X, Chen Y, Li L, Wei Z, Deng H, Liu J, Frederiksen NA *et al* (2021) Two cGAS-like receptors induce antiviral immunity in *Drosophila*. *Nature* 597: 114–118

Imai Y, Matsuo N, Ogawa S, Tohyama M, Takagi T (1998) Cloning of a gene, YT521, for a novel RNA splicing-related protein induced by hypoxia/reoxygenation. *Mol Brain Res* 53: 33–40

Imam H, Khan M, Gokhale NS, McIntyre ABR, Kim G-W, Jang JY, Kim S-J, Mason CE, Horner SM, Siddiqui A (2018) N6-methyladenosine modification of hepatitis B virus RNA differentially regulates the viral life cycle. *Proc Natl Acad Sci USA* 115: 8829–8834

Jin Y, Zhao JH, Guo HS (2021) Recent advances in understanding plant antiviral RNAi and viral suppressors of RNAi. *Curr Opin Virol* 46: 65–72

Jurczyszak D, Zhang W, Terry SN, Kehrer T, Bermúdez González MC, McGregor E, Mulder LCF, Eckwahl MJ, Pan T, Simon V (2020) HIV protease cleaves the antiviral m6A reader protein YTHDF3 in the viral particle. *PLoS Pathog* 16: e1008305

Kawai Y, Ono E, Mizutani M (2014) Evolution and diversity of the 2-oxoglutarate-dependent dioxygenase superfamily in plants. *Plant J* 78: 328−343

Kennedy EM, Bogerd HP, Kornepati AVR, Kang D, Ghoshal D, Marshall JB, Poling BC, Tsai K, Gokhale NS, Horner SM *et al* (2016) Posttranscriptional m6A editing of HIV-1 mRNAs enhances viral gene expression. *Cell Host Microbe* 19: 675−685

Kierzek E, Kierzek R (2003) The thermodynamic stability of RNA duplexes and hairpins containing N6-alkyladenosines and 2-methylthio-N6-alkyladenosines. *Nucleic Acids Res* 31: 4472−4480

Kontur C, Jeong M, Cifuentes D, Giraldez AJ (2020) Ythdf m6A readers function redundantly during zebrafish development. *Cell Rep* 33: 108598

Koopal B, Potocnik A, Mutte SK, Aparicio-Maldonado C, Lindhoud S, Vervoort JJM, Brouns SJJ, Swarts DC (2022) Short prokaryotic Argonaute systems trigger cell death upon detection of invading DNA. *Cell* 185: 1471−1486

Lasman L, Krupalnik V, Viukov S, Mor N, Aguilera-Castrejon A, Schneir D, Bayerl J, Mizrahi O, Peles S, Tawil S *et al* (2020) Context-dependent compensation between functional Ythdf m6A reader proteins. *Genes Dev* 34: 1373−1391

Lavi S, Shatkin AJ (1975) Methylated simian virus 40-specific RNA from nuclei and cytoplasm of infected BSC-1 cells. *Proc Natl Acad Sci USA* 72: 2012−2016

Le Pen J, Jiang H, Di Domenico T, Kneuss E, Kosałka J, Leung C, Morgan M, Much C, Rudolph KLM, Enright AJ *et al* (2018) Terminal uridylyltransferases target RNA viruses as part of the innate immune system. *Nat Struct Mol Biol* 25: 778−786

Li F, Zhao D, Wu J, Shi Y (2014) Structure of the YTH domain of human YTHDF2 in complex with an m6A mononucleotide reveals an aromatic cage for m6A recognition. *Cell Res* 24: 1490−1492

Liao S, Sun H, Xu C (2018) YTH domain: a family of N6-methyladenosine (m6A) readers. *Genomics Proteomics Bioinformatics* 16: 99−107

Lichinchi G, Zhao BS, Wu Y, Lu Z, Qin Y, He C, Rana TM (2016) Dynamics of human and viral RNA methylation during Zika virus infection. *Cell Host Microbe* 20: 666−673

Lilly ST, Drummond RSM, Pearson MN, MacDiarmid RM (2011) Identification and validation of reference genes for normalization of transcripts from virus-infected *Arabidopsis thaliana*. *Mol Plant Microbe Interact* 24: 294−304

Lindbo JA (2012) A historical overview of RNAi in plants. *Methods Mol Biol* 894: 1−16

Liu N, Dai Q, Zheng G, He C, Parisien M, Pan T (2015) N6-methyladenosine-dependent RNA structural switches regulate RNA-protein interactions. *Nature* 518: 560−564

Loenen WAM, Dryden DTF, Raleigh EA, Wilson GG, Murrayy NE (2014) Highlights of the DNA cutters: a short history of the restriction enzymes. *Nucleic Acids Res* 42: 3−19

Lopez-Gomollon S, Baulcombe DC (2022) Roles of RNA silencing in viral and non-viral plant immunity and in the crosstalk between disease resistance systems. *Nat Rev Mol Cell Biol* 23: 645−662

Luo S, Tong L (2014) Molecular basis for the recognition of methylated adenines in RNA by the eukaryotic YTH domain. *Proc Natl Acad Sci USA* 111: 13834−13839

Ma W, Cui S, Lu Z, Yan X, Cai L, Lu Y, Cai K, Zhou H, Ma R, Zhou S *et al* (2022) YTH domain proteins play an essential role in Rice growth and stress response. *Plan Theory* 11: 2206

Marquez-Molins J, Juarez-Gonzalez VT, Gomez G, Pallas V, Martinez G (2022) Occurrence of RNA post-transcriptional modifications in plant viruses and viroids and their correlation with structural and functional features. *Virus Res* 323: 198958

Martin EW, Holehouse AS, Peran I, Farag M, Incicco JJ, Bremer A, Grace CR, Soranno A, Pappu RV, Mittag T (2020) Valence and patterning of aromatic residues determine the phase behavior of prion-like domains. *Cell* 376: 694−699

Martínez-Pérez M, Aparicio F, López-Gresa MP, Bellés JM, Sánchez-Navarro JA, Pallás V (2017) *Arabidopsis* m6A demethylase activity modulates viral infection of a plant virus and the m6A abundance in its genomic RNAs. *Proc Natl Acad Sci USA* 114: 10755−10760

Martínez-Pérez M, Gómez-Mena C, Alvarado-Marchena L, Nadi R, Micol JL, Pallas V, Aparicio F (2021) The m6A RNA demethylase ALKBH9B plays a critical role for vascular movement of alfalfa mosaic virus in *Arabidopsis*. *Front Microbiol* 12: 745576

McMahon AC, Rahman R, Jin H, Shen JL, Fieldsend A, Luo W, Rosbash M (2016) TRIBE: hijacking an RNA-editing enzyme to identify cell-specific targets of RNA-binding proteins. *Cell* 165: 742−753

Meier N, Hatch C, Nagalakshmi U, Dinesh-Kumar SP (2019) Perspectives on intracellular perception of plant viruses. *Mol Plant Pathol* 20: 1185−1190

Mielecki D, Zugaj D, Muszewska A, Piwowarski J, Chojnacka A, Mielecki M, Nieminuszczy J, Grynberg M, Grzesiuk E (2012) Novel AlkB dioxygenases-alternative models for in silico and in vivo studies. *PLoS ONE* 7: e30588

Mourrain P, Béclin C, Elmayan T, Feuerbach F, Godon C, Morel JB, Jouette D, Lacombe AM, Nikic S, Picault N *et al* (2000) *Arabidopsis* SGS2 and SGS3 genes are required for posttranscriptional gene silencing and natural virus resistance. *Cell* 101: 533−542

Murakami S, Jaffrey SR (2022) Hidden codes in mRNA: control of gene expression by m6A. *Mol Cell* 82: 2236−2251

Niehl A, Heinlein M (2019) Perception of double-stranded RNA in plant antiviral immunity. *Mol Plant Pathol* 20: 1203−1210

Nour-Eldin HH, Hansen BG, Nørholm MHH, Jensen JK, Halkier BA (2006) Advancing uracil-excision based cloning towards an ideal technique for cloning PCR fragments. *Nucleic Acids Res* 34: e122

Pallás V, Más P, Sánchez-Navarro JA (1998) Detection of plant RNA viruses by nonisotopic dot-blot hybridization. *Methods Mol Biol* 81: 461−468

Pallas V, Aparicio F, Herranz MC, Sanchez-Navarro JA, Scott SW (2013) The molecular biology of Ilarviruses. *Adv Virus Res* 87: 139−181

Patil DP, Pickering BF, Jaffrey SR (2018) Reading m6A in the transcriptome: m6A-binding proteins. *Trends Cell Biol* 28: 113−127

Patro R, Duggal G, Love MI, Irizarry RA, Kingsford C (2017) Salmon provides fast and bias-aware quantification of transcript expression. *Nat Methods* 14: 417−419

Popp MWL, Cho H, Maquat LE (2020) Viral subversion of nonsense-mediated mRNA decay. *RNA* 26: 1509−1518

Postnikova OA, Nemchinov LG (2012) Comparative analysis of microarray data in *Arabidopsis* transcriptome during compatible interactions with plant viruses. *Virol J* 29: 101

Poulsen LD, Kielpinski LJ, Salama SR, Krogh A, Vinther J (2015) SHAPE selection (SHAPES) enrich for RNA structure signal in SHAPE sequencing-based probing data. *RNA* 21: 1042−1052

Qi Y, Denli AM, Hannon GJ (2005) Biochemical specialization within *Arabidopsis* RNA silencing pathways. *Mol Cell* 19: 421−428

R Core Team (2021) *R: a language and environment for statistical computing*. Vienna, Austria: R Foundation for Statistical Computing https://www.R-project.Org/

Rehwinkel J, Gack MU (2020) RIG-I-like receptors: their regulation and roles in RNA sensing. *Nat Rev Immunol* 20: 537–551

Rennie S, Heidar Magnusson D, Andersson R (2021) hyperTRIBER: a flexible R package for the analysis of differential RNA editing. *bioRxiv* https://doi.org/10.1101/2021.10.20.465108 [PREPRINT]

Ries RJ, Zaccara S, Klein P, Olarerin-George A, Namkoong S, Pickering BF, Patil DP, Kwak H, Lee JH, Jaffrey SR (2019) m6A enhances the phase separation potential of mRNA. *Nature* 571: 424–428

Růžička K, Zhang M, Campilho A, Bodi Z, Kashif M, Saleh M, Eeckhout D, El-Showk S, Li H, Zhong S *et al* (2017) Identification of factors required for m6A mRNA methylation in *Arabidopsis* reveals a role for the conserved E3 ubiquitin ligase HAKAI. *New Phytol* 215: 157–172

Sacco MT, Bland KM, Horner SM (2022) WTAP targets the METTL3 m6A-Methyltransferase complex to cytoplasmic hepatitis C virus RNA to regulate infection. *J Virol* 96: e0099722

Sambrook J, Maniatis T, Fritsch EF (1988) *Molecular cloning: a laboratory manual*, 2nd edn. New York, NY: Cold Spring Harbor Laboratory

Scutenaire J, Deragon J-M, Jean V, Benhamed M, Raynaud C, Favory J-J, Merret R, Bousquet-Antonelli C (2018) The YTH domain protein ECT2 is an m6A reader required for Normal Trichome branching in *Arabidopsis*. *Plant Cell* 30: 986–1005

Shen L, Liang Z, Gu X, Chen Y, Teo ZWN, Hou X, Cai WM, Dedon PC, Liu L, Yu H (2016) N6-methyladenosine RNA modification regulates shoot stem cell fate in *Arabidopsis*. *Dev Cell* 38: 186–200

Slavik KM, Morehouse BR, Ragucci AE, Zhou W, Ai X, Chen Y, Li L, Wei Z, Bähre H, König M *et al* (2021) cGAS-like receptors sense RNA and control 3′2′-cGAMP signalling in *Drosophila*. *Nature* 597: 109–113

Srinivas KP, Depledge DP, Abebe JS, Rice SA, Mohr I, Wilson AC (2021) Widespread remodeling of the m6A RNA-modification landscape by a viral regulator of RNA processing and export. *Proc Natl Acad Sci USA* 118: e2104805118

Stoilov P, Rafalska I, Stamm S (2002) YTH: a new domain in nuclear proteins. *Trends Biochem Sci* 27: 495–497

Tal N, Morehouse BR, Millman A, Stokar-Avihail A, Avraham C, Fedorenko T, Yirmiya E, Herbst E, Brandis A, Mehlman T *et al* (2021) Cyclic CMP and cyclic UMP mediate bacterial immunity against phages. *Cell* 184: 5728–5739

Tankmar MD, Reichel M, Arribas-Hernandez L, Brodersen P (2023) A YTHDF-PABP axis is required for m6A-mediated organogenesis in plants. *bioRxiv* https://doi.org/10.1101/2023.07.03.547513 [PREPRINT]

Tesei G, Lindorff-Larsen K (2023) Improved predictions of phase behaviour of intrinsically disordered proteins by tuning the interaction range. *Open Res Eur* 2: 94

Tesei G, Schulze TK, Crehuet R, Lindorff-Larsen K (2021) Accurate model of liquid–liquid phase behavior of intrinsically disordered proteins from optimization of single-chain properties. *Proc Natl Acad Sci USA* 118: e2111696118

Theler D, Dominguez C, Blatter M, Boudet J, Allain FHT (2014) Solution structure of the YTH domain in complex with N6-methyladenosine RNA: a reader of methylated RNA. *Nucleic Acids Res* 42: 13911–13919

Tian S, Wu N, Zhang L, Wang X (2021) RNA N6-methyladenosine modification suppresses replication of rice black streaked dwarf virus and is associated with virus persistence in its insect vector. *Mol Plant Pathol* 22: 1070–1081

Tirumuru N, Zhao BS, Lu W, Lu Z, He C, Wu L (2016) N6-methyladenosine of HIV-1 RNA regulates viral infection and HIV-1 gag protein expression. *Elife* 5: e15528

Tsutsui H, Higashiyama T (2017) PKAMA-ITACHI vectors for highly efficient CRISPR/Cas9-mediated gene knockout in *Arabidopsis thaliana*. *Plant Cell Physiol* 58: 46–56

van den Born E, Omelchenko MV, Bekkelund A, Leihne V, Koonin EV, Dolja VV, Falnes PO (2008) Viral AlkB proteins repair RNA damage by oxidative demethylation. *Nucleic Acids Res* 36: 5451–5461

van den Born E, Bekkelund A, Moen MN, Omelchenko MV, Klungland A, Falnes P (2009) Bioinformatics and functional analysis define four distinct groups of AlkB DNA-dioxygenases in bacteria. *Nucleic Acids Res* 37: 7124–7136

Vaucheret H, Vazquez F, Crété P, Bartel DP (2004) The action of ARGONAUTE1 in the miRNA pathway and its regulation by the miRNA pathway are crucial for plant development. *Genes Dev* 18: 1187–1197

Voinnet O, Pinto YM, Baulcombe DC (1999) Suppression of gene silencing: a general strategy used by diverse DNA and RNA viruses of plants. *Proc Natl Acad Sci USA* 96: 14147–14152

Wang XB, Jovel J, Udomporn P, Wang Y, Wu Q, Li WX, Gasciolli V, Vaucheret H, Ding SW (2011) The 21-nucleotide, but not 22-nucleotide, viral secondary small interfering RNAs direct potent antiviral defense by two cooperative argonautes in *Arabidopsis thaliana*. *Plant Cell* 23: 1625–1638

Wang J, Choi JM, Holehouse AS, Lee HO, Zhang X, Jahnel M, Maharana S, Lemaitre R, Pozniakovsky A, Drechsel D *et al* (2018) A molecular grammar governing the driving forces for phase separation of prion-like RNA binding proteins Jie. *Cell* 176: 688–699

Wiener D, Schwartz S (2021) The epitranscriptome beyond m6A. *Nat Rev Genet* 22: 119–131

Williams GD, Gokhale NS, Horner SM (2019) Regulation of viral infection by the RNA modification N6-Methyladenosine. *Annu Rev Virol* 6: 235–253

Wu J, Chen ZJ (2014) Innate immune sensing and signaling of cytosolic nucleic acids. *Annu Rev Immunol* 32: 461–488

Wu F, Cheng W, Zhao F, Tang M, Diao Y, Xu R (2020) Association of N6-methyladenosine with viruses and virally induced diseases. *Front Biosci (Landmark Ed)* 25: 1184–1201

Xu C, Wang X, Liu K, Roundtree IA, Tempel W, Li Y, Lu Z, He C, Min J (2014) Structural basis for selective binding of m6A RNA by the YTHDC1 YTH domain. *Nat Chem Biol* 10: 927–929

Xu C, Liu K, Ahmed H, Loppnau P, Schapira M, Min J (2015) Structural basis for the discriminative recognition of N6-Methyladenosine RNA by the human YT521-B homology domain family of proteins. *J Biol Chem* 290: 24902–24913

Xu W, Rahman R, Rosbash M (2018) Mechanistic implications of enhanced editing by a HyperTRIBE RNA-binding protein. *RNA* 24: 173–182

Yin S, Qiujing A, Qiu T, Tan C, Tu Y, Kuang T, Yang Y (2022) Tomato SlYTH1 encoding a putative RNA m6A reader affects plant growth and fruit shape. *Plant Sci* 323: 111417

Zhang Z, Theler D, Kaminska KH, Hiller M, De La Grange P, Pudimat R, Rafalska I, Heinrich B, Bujnick JM, Allain FHT *et al* (2010) The YTH domain is a novel RNA binding domain. *J Biol Chem* 285: 14701–14710

Zhang TY, Wang ZQ, Hu HC, Chen ZQ, Liu P, Gao SQ, Zhang F, He L, Jin P, Xu MZ *et al* (2021) Transcriptome-wide N6-Methyladenosine (m6A) profiling of susceptible and resistant wheat varieties reveals the involvement of variety-specific m6A modification involved in virus-host interaction pathways. *Front Microbiol* 12: 656302

Zhang M, Bodi Z, Mackinnon K, Zhong S, Archer N, Mongan NP, Simpson GG, Fray RG (2022a) Two zinc finger proteins with functions in m6A writing interact with HAKAI. *Nat Commun* 13: 1127

Zhang T, Shi C, Hu H, Zhang Z, Wang Z, Chen Z, Feng H, Liu P, Guo J, Lu Q *et al* (2022b) N6-methyladenosine RNA modification promotes viral genomic RNA stability and infection. *Nat Commun* 13: 6576

Zhong S, Li H, Bodi Z, Button J, Vespa L, Herzog M, Fray RG (2008) MTA is an *Arabidopsis* messenger RNA adenosine Methylase and interacts with a homolog of a sex-specific splicing factor. *Plant Cell Online* 20: 1278–1288

Zhu T, Roundtree IA, Wang P, Wang X, Wang L, Sun C, Tian Y, Li J, He C, Xu Y (2014) Crystal structure of the YTH domain of YTHDF2 reveals mechanism for recognition of N6-methyladenosine. *Cell Res* 24: 1493–1496